

# Sequential Detection and Estimation of Multipath Channel Parameters Using Belief Propagation

Xuhong Li\*, *Student Member, IEEE*, Erik Leitinger†, *Member, IEEE*,  
 Alexander Venus†, *Student Member, IEEE*, and Fredrik Tufvesson\*, *Fellow, IEEE*,

## Abstract

This paper proposes a belief propagation (BP)-based algorithm for sequential detection and estimation of multipath components (MPCs) parameters based on radio signals. Under dynamic channel conditions with moving transmitter and/or receiver, the number of MPCs reflected from visible geometric features, the MPC dispersion parameters (delay, angle, Doppler frequency, etc), and the number of false alarm contributions are unknown and time-varying. We develop a Bayesian model for sequential detection and estimation of MPC dispersion parameters, and represent it by a factor graph enabling the use of BP for efficient computation of the marginal posterior distributions. At each time instance, a snapshot-based channel estimator provides parameter estimates of a set of MPCs which are used as noisy measurements by the proposed BP-based algorithm. It performs joint probabilistic data association, estimation of the time-varying MPC parameters, and the mean number of false alarm measurements by means of the sum-product algorithm rules. The results using synthetic measurements show that the proposed algorithm is able to cope with a high number of false alarm measurements originating from the snapshot-based channel estimator and to sequentially detect and estimate MPCs parameters with very low signal-to-noise ratio (SNR). The performance of the proposed algorithm compares well to existing algorithms for high SNR MPCs, but significantly it outperforms them for medium or low SNR MPCs. In particular, we show that our algorithm outperforms the Kalman enhanced super resolution tracking (KEST) algorithm, a state-of-the-art sequential channel parameters estimation method. Furthermore, results with real radio measurements demonstrate the excellent performance of the algorithm in realistic and challenging scenarios.

## I. INTRODUCTION

The information of dispersive wireless radio channels and its temporal behavior in dynamic scenarios are of great importance for the design and development of radio-channel models

X. Li, and F. Tufvesson are with the Department of Electrical and Information Technology, Lund University, Sweden (e-mail: xuhong.li, fredrik.tufvesson@eit.lth.se). E. Leitinger and A. Venus are with the Laboratory of Signal Processing and Speech Communication, Graz University of Technology, Austria and the Christian Doppler Laboratory for Location-aware Electronic Systems (e-mail: {erik.leitinger, a.venus}@tugraz.at). This work was supported in part by the Swedish Research Council (VR), in part by the strategic research area ELLIIT, in part by the Christian Doppler Research Association and in part by the TU Graz.

[1], [2], 5G wireless communication technologies [3]–[5], and multipath-based localization and mapping [6]–[9]. The response of a non-static wireless radio channel is typically represented by superimposed weighted Dirac delta distributions with distinct and time-varying locations (or supports) in the respective dispersion domains (delay, angle of arrival (AoA), angle of departure (AoD), Doppler frequency, and combinations thereof). Each component is meant to represent a multipath component (MPC). In general, the channel response can be observed only within a finite aperture leading to some limitations on the ability to resolve MPCs closely spaced in the dispersion domains. The related time-varying MPC parameters are usually estimated from multidimensional radio measurements using antenna arrays and multiple frequencies (wideband or ultra-wideband) using super resolution (SR) algorithms that perform sequential estimation of MPC parameters.

### A. State-of-the-Art Methods

If the number of MPCs is known, subspace methods [10]–[12] or maximum likelihood (ML) methods as for example [13] are standard super-resolution methods to estimate time-invariant MPC parameters. Expectation maximization-based methods [14], have proven a viable approximation of the computationally prohibitive ML methods [15]. In recent years, a channel model has been introduced that also considers a dense multipath component (DMC) [16]. The DMC incorporates MPCs that cannot be resolved due to finite observation aperture. Including the estimation of DMC can improve the accuracy of the parameter estimation of distinct MPCs.

All afore-mentioned methods have in common that they do not incorporate the estimation of the number of MPCs i.e., model order, into the estimation problem. One classical solution is to extend the methods with an outer stage for model order detection using for example eigenvalue-based methods, or the generic information theoretic criteria, e.g., the Akaike/Bayesian information criterion, the minimum description length (MDL) principle [17]. The outer stage schemes mostly tend to overestimate the model order. Inspired by the ideas of sparse estimation and compressed sensing, some super-resolution sparse Bayesian parametric channel estimation algorithms [18]–[21] have recently appeared which aim to reconstruct sparse signals from a reduced set of measurements specified by a sparse weight vector. By introducing a sparsity-promoting prior model for the weights, the estimation of the number of MPCs and their parameters can be jointly formulated in a Bayesian framework.

In order to capture the temporal behavior of MPC parameters in time-varying scenarios, many sequential estimation methods have been proposed, which can be grouped into two broad categories. Methods of the first category sequentially estimate the MPC parameters directly based on the radio signals using for example an extended Kalman filter [22]–[24]. Methods of the second category are based on a two-stage approach, where the estimates of a snapshot-based channel estimator are used as noisy measurements in a tracking filter [25]. In this work, we focus on the two-stage methods. Due to the finite aperture of measurement systems and resolution capability of snapshot-based parametric channel estimators, some measurements for the second stage might incorporate contributions from more than one MPC and false alarms may exist. In this case, to decide which measurement should be used for the update of which MPC (i.e., data association (DA) problem) can be complicated. In general, existing sequential channel estimation methods adopt “hard” association which assumes that the measurements are fine resolved and each of them originates from single MPC that is specified by metrics such as the global nearest neighbor [26]. Probabilistic DA [26], [27], on the other hand, solves the origin uncertainty problem in a “soft” manner, in which the association probabilities for all current measurements are computed and used to form a mixture probability density function (PDF) for the update of each MPC’s state.

### *B. Contributions and Paper Organization*

Here, we propose a belief propagation (BP)-based algorithm for MPC sequential detection and estimation (SDE) of their dispersion parameters (abbreviated as BP-MPC-SDE algorithm) that uses the MPC estimates from a snapshot-based parametric SR-sparse Bayesian learning (SBL) channel estimator as measurements (abbreviated as SR-SBL). This BP-MPC-SDE algorithm jointly performs probabilistic DA and sequential estimation of potential MPC (PMPC) parameters by running the BP algorithm, also known as the sum-product algorithm (SPA), on a factor graph [8], [27]–[29]. Note that independence between MPCs is assumed throughout the work, therefore correlation information is negligible. We use a probabilistic model for MPC existence where each PMPC state is augmented by a binary existence variable and associated with a probability of existence, which is also estimated and used for detection of the reliable MPCs modeling the birth and death of these components [8], [30]. Inspired by [31]–[33], the algorithm also exploits the amplitude statistic of the measurements to determine the detection probabilities related to the PMPCs’ states. It is therefore also suitable for unknown and time-varying detection probabilities

[32]–[34]. Incorporating amplitude information helps to improve the detectability and increase the lifetimes of “weak” MPCs with low SNRs. Moreover, by exploring different amplitude distributions of MPC-oriented measurements and false alarm measurements, the algorithm can better discriminate against false alarms. Further, the proposed algorithm estimates the possibly time-varying mean false alarm rate (FAR) to cope with false alarm measurements originating from the preprocessing step and clutter measurements originating from strongly fluctuating MPCs (for example DMC or short-lived scatter components). The main contributions of this paper are summarized as follows.

- We introduce a Bayesian model for sequential detection and estimation of MPC parameters, which use the estimates from a snapshot-based channel estimator as measurements. Within this model, the death and birth of MPCs and DAs are formulated probabilistically, and adaptive detection probabilities are incorporated by exploiting amplitude information.
- We further present a BP algorithm based on the factor graph representation of the estimation problem, where the states of MPCs, and the mean FAR are estimated jointly and sequentially. The algorithm exhibits very good scalability in the numbers of measurements as well as the number of PMPCs.
- The performance of the proposed algorithm is demonstrated with both synthetic and real measurements. In particular, the results using synthetic measurements are compared with the KEST [25] algorithm (a state-of-the-art sequential channel parameters estimation method), and posterior Cramér–Rao lower bound (CRLB) (PCRLB).

The remainder of this paper is organized as follows. Section II outlines the underlying radio signal model and the snapshot-based SR-SBL channel estimator. Section III gives system models and statistical formulations of the MPC sequential detection and estimation problem. Section IV presents the joint posterior PDF and factor graph. In Section V, we develop the BP-MPC-SDE algorithm. Experimental results using synthetic and real measurements are presented in Section VI. Section VII concludes the paper.

*Notations:* Column vectors and matrices are denoted by boldface lowercase and uppercase letters. Random variables are displayed in san serif, upright fonts as for example  $\mathbf{x}$  and  $\mathbf{X}$  and their realizations in serif, italic font as for example  $x$  and  $\mathbf{x}$ .  $f(\mathbf{x})$  denotes the PDF or probability mass function (PMF) of continuous or discrete random vector.  $(\cdot)^T$ ,  $(\cdot)^*$ , and  $(\cdot)^H$  denote matrix transpose, complex conjugation and Hermitian transpose, respectively.  $\|\cdot\|$  is the Euclidean norm.  $|\cdot|$  represents the cardinality of a set.  $\text{diag}\{\mathbf{x}\}$  denotes a diagonal matrix with entries in  $\mathbf{x}$ .  $\text{tr}\{\cdot\}$

denotes the trace of a matrix.  $\mathbf{I}_{[\cdot]}$  is an identity matrix of dimension given in the subscript.  $[\mathbf{X}]_{n,n}$  denotes the  $n$ th diagonal entry of  $\mathbf{X}$ .  $[\mathbf{X}]_{1:n}$  denotes a sub-matrix containing  $1:n$  columns and rows of  $\mathbf{X}$ . Furthermore,  $\bar{1}(e)$  denotes the function of the event  $e = 0$  (i.e.,  $\bar{1}(e) = 1$  if  $e = 0$  and 0 otherwise).  $1_{\mathbb{A}}(\mathbf{x})$  denotes the indicator function that is  $1_{\mathbb{A}}(\mathbf{x}) = 1$  if  $\mathbf{x} \in \mathbb{A}$  and 0 otherwise. For any function  $g(\mathbf{x})$  we define the integral  $\langle g(\mathbf{x}) \rangle_{f(\mathbf{x})} = \int g(\mathbf{x})f(\mathbf{x})d\mathbf{x}$ . As for example  $\langle \mathbf{x} \rangle_{f(\mathbf{x})} = \int \mathbf{x}f(\mathbf{x})d\mathbf{x}$  and  $\langle f(\mathbf{x}) \rangle_{1_{\mathbb{A}}(\mathbf{x})} = \int_{\mathbb{A}} f(\mathbf{x})d\mathbf{x}$  denote the expected value and the integral over  $f(\mathbf{x})$  of the random vector  $\mathbf{x}$ , respectively.

## II. RADIO SIGNAL MODEL

We consider a single-input-multiple-output (SIMO) ultra-wideband measurement equipment. A baseband radio signal  $s(t)$  is transmitted from a base station (BS) equipped with a single antenna to a mobile user (UE) equipped with an antenna array of  $H$  elements located at  $\mathbf{p}^{(h)} \in \mathbb{R}^{2 \times 1}$  with  $h \in \{1, \dots, H\}$ .<sup>1</sup> We define  $d^{(h)} = \|\mathbf{p}^{(h)} - \mathbf{p}\|$  and  $\varphi^{(h)} = \angle(\mathbf{p}^{(h)} - \mathbf{p}) - \psi$ , the distance of the  $h$ -th element to the reference location  $\mathbf{p} \in \mathbb{R}^{2 \times 1}$ , i.e., the center of gravity of the array, and its angle relative to the array orientation  $\psi$ , respectively. For the sake of brevity, we assume a two dimensional scenario with horizontal-only propagation.<sup>2</sup>

### A. Received Signal

Signals are represented by their complex envelope with respect to a center frequency  $f_c$ . The received signal at each antenna element  $h$  at the discrete observation time  $n$  is given as

$$s_{\text{RX},n}^{(h)}(t) = \sum_{l=1}^{L_n} \tilde{\alpha}_{l,n} s(t; \tilde{d}_{l,n}, \tilde{\varphi}_{l,n}, \mathbf{p}^{(h)}) + w_n^{(h)}(t) \quad (1)$$

where the first term comprises  $L_n$  MPCs, with each being characterized by its complex amplitude  $\tilde{\alpha}_{l,n} \in \mathbb{C}$ , the distance  $\tilde{d}_{l,n} = c\tilde{\tau}_{l,n} \in \mathbb{R}$  to the array's center of gravity directly related to the time delay via the speed of light  $c$ , and the AoA  $\tilde{\varphi}_{l,n} \in [-\pi, \pi)$  with respect to the array orientation. Under the far-field plane-wave assumption, the signal  $s(t; \tilde{d}, \tilde{\varphi}, \mathbf{p}^{(h)})$  is given as  $s(t; \tilde{d}, \tilde{\varphi}, \mathbf{p}^{(h)}) = e^{j2\pi f_c g(\tilde{\varphi}, \mathbf{p}^{(h)})} \tilde{s}(t - \tilde{d}/c + g(\tilde{\varphi}, \mathbf{p}^{(h)}))$  with  $\tilde{s}(t)$  as the transmitted signal pulse. The function  $g(\tilde{\varphi}, \mathbf{p}^{(h)}) = \frac{d^{(h)} \cos(\tilde{\varphi} - \psi - \varphi^{(h)})}{c}$  gives the delay shift of a plane wave incident with

<sup>1</sup>Note that the extension of the algorithm to a multiple-input-multiple-output (MIMO) system considering an antenna array at the BS as well is straightforward.

<sup>2</sup>An extension to three-dimensional scenarios with horizontal and vertical propagation is straightforward, but it would lead to a cumbersome notation and one would not gain any new insights.

AoA  $\tilde{\varphi}$  being measured relative to the array orientation  $\psi$ , at the  $h$ th antenna position with respect to the array center of gravity. We assume that the UE and BS are time synchronized and the array orientation is known. The measurement noise processes  $w_n^{(h)}(t)$  in (1) are independent additive white Gaussian noise (AWGN) with double-sided power spectral density  $N_0/2$ .

The received signal in (1) observed over a duration  $T$  is sampled with frequency  $f_s = 1/T_s$  at each time  $n$ , yielding a length  $N_s = T/T_s$  sample vector  $\mathbf{s}_{\text{RX},n}^{(h)} \in \mathbb{C}^{N_s \times 1}$  from each array element. By stacking  $\mathbf{s}_{\text{RX},n}^{(h)}$  from  $H$  array elements, the discrete time signal vector  $\mathbf{s}_{\text{RX},n} \triangleq [\mathbf{s}_{\text{RX},n}^{(1)\text{T}} \cdots \mathbf{s}_{\text{RX},n}^{(H)\text{T}}]^{\text{T}} \in \mathbb{C}^{N_s H \times 1}$  is given by

$$\mathbf{s}_{\text{RX},n} = \mathbf{S}(\tilde{\boldsymbol{\theta}}_n) \tilde{\boldsymbol{\alpha}}_n + \mathbf{w}_n. \quad (2)$$

In the first summand  $\tilde{\boldsymbol{\alpha}}_n^{\text{T}} \triangleq [\tilde{\alpha}_{1,n} \cdots \tilde{\alpha}_{L_n,n}]^{\text{T}} \in \mathbb{C}^{L_n \times 1}$ ,  $\tilde{\boldsymbol{\theta}}_n \triangleq [\tilde{\boldsymbol{\theta}}_{1,n}^{\text{T}} \cdots \tilde{\boldsymbol{\theta}}_{L_n,n}^{\text{T}}]^{\text{T}} \in \mathbb{R}^{2L_n \times 1}$  with  $\tilde{\boldsymbol{\theta}}_{l,n} \triangleq [\tilde{d}_{l,n}, \tilde{\varphi}_{l,n}]^{\text{T}} \in \mathbb{R}^{2 \times 1}$  denoting the vector comprising the MPC parameters and  $\mathbf{S}(\tilde{\boldsymbol{\theta}}_n) \triangleq [\mathbf{s}(\tilde{\boldsymbol{\theta}}_{1,n}) \cdots \mathbf{s}(\tilde{\boldsymbol{\theta}}_{L_n,n})] \in \mathbb{C}^{N_s H \times L_n}$  with columns given by  $\mathbf{s}(\tilde{\boldsymbol{\theta}}_{l,n}) = [\mathbf{s}_1(\tilde{\boldsymbol{\theta}}_{l,n})^{\text{T}} \cdots \mathbf{s}_H(\tilde{\boldsymbol{\theta}}_{l,n})^{\text{T}}]^{\text{T}} \in \mathbb{C}^{N_s H \times 1}$ . The  $h$ th entry of  $\mathbf{s}(\tilde{\boldsymbol{\theta}}_{l,n})$  reads  $\mathbf{s}_h(\tilde{\boldsymbol{\theta}}_{l,n}) \triangleq [s(-[(N-1)/2]T_s; \tilde{d}_{l,n}, \tilde{\varphi}_{l,n}, \mathbf{p}^{(h)}) \cdots s([(N-1)/2]T_s; \tilde{d}_{l,n}, \tilde{\varphi}_{l,n}, \mathbf{p}^{(h)})]^{\text{T}} \in \mathbb{C}^{N_s \times 1}$ . The measurement noise vector  $\mathbf{w}_n \in \mathbb{C}^{N_s H \times 1}$  is a complex circular symmetric Gaussian random vector with covariance matrix  $\mathbf{C} = \sigma^2 \mathbf{I}_{N_s H}$  where  $\sigma^2 = N_0/T_s$  is the noise variance. The component SNR of each MPC is given by  $\text{SNR}_{l,n} = \frac{|\tilde{\alpha}_{l,n}|^2 \|\mathbf{s}(\tilde{\boldsymbol{\theta}}_{l,n})\|^2}{\sigma^2}$  and the according normalized amplitude by  $\tilde{u}_{l,n} = \sqrt{\text{SNR}_{l,n}}$ . A MPC exists only during the time duration that the associated geometric feature is visible (i.e., lifetime) at the UE position. The true number  $L_n$  of MPCs as well as their individual parameters  $\tilde{u}_{l,n}$ ,  $\tilde{d}_{l,n}$ , and  $\tilde{\varphi}_{l,n}$  are unknown and time-varying in dynamic scenarios. In this paper we propose an algorithm to sequentially detect and estimate these parameters.

### B. Parametric Channel Estimation

At each time  $n$ , a snapshot-based SR-SBL estimator [18]–[21], [35] provides estimated dispersion parameters of  $M_n$  MPCs stacked into the vector  $\mathbf{z}_n \triangleq [\mathbf{z}_{1,n}^{\text{T}} \cdots \mathbf{z}_{M_n,n}^{\text{T}}]^{\text{T}} \in \mathbb{R}^{3M_n \times 1}$ , where  $\mathbf{z}_{m,n} \triangleq [z_{\text{d},m,n} \ z_{\varphi,m,n} \ z_{\text{u},m,n}]^{\text{T}} \in \mathbb{R}^{3 \times 1}$  comprises estimates of the distance  $z_{\text{d},m,n} = \hat{d}_{m,n}$ , the AoA  $z_{\varphi,m,n} = \hat{\varphi}_{m,n}$ , and the normalized amplitude  $z_{\text{u},m,n} = \hat{u}_{m,n}$  as well as the noise variance  $\hat{\sigma}^2$ .

The normalized amplitude estimate is given by  $\hat{u}_{m,n} \triangleq |\mu_{m,n}| / \sqrt{[\Sigma_{\mu_n}]_{m,m}}$  where  $\mu_{m,n}$  and  $\Sigma_{\mu_n}$ , respectively, denote the estimated mean and covariance matrix of the MPC complex amplitudes. Note that the amplitudes are directly related to the detection probabilities of the estimated MPCs [32], [33] (see for Section III-C). At time  $n = 1$ , the initial prior PDF  $f(\mathbf{z}_{m,1})$  of the

dispersion parameters in the snapshot-based estimator is considered as uniform in the validation region. For each time  $n \geq 2$ , the snapshot-based estimator is initialized by  $\hat{L}_{n-1}$  detected MPCs from the BP-MPC-SDE algorithm at time  $n-1$ . Specifically, the PDF  $f(z_{m,n})$  is assumed to be Gaussian with mean vector given by the minimum mean-square error (MMSE) estimate of the parameters  $\theta_{k,n-1}^{\text{MMSE}} \in \mathbb{R}^{2 \times 1}$  and covariance matrix  $\Sigma_{k,n-1} = \text{diag}\{[\{\sigma_{d_{k,n-1}}^{\text{MMSE}} \ \sigma_{\varphi_{k,n-1}}^{\text{MMSE}}]^T\} \in \mathbb{R}^{2 \times 2}$  with  $k \in \{1, \dots, \hat{L}_{n-1}\}$  (see for Section IV-B).

The vector  $z_n$  is used as noisy measurement in the BP-MPC-SDE algorithm.

### III. SYSTEM MODEL

#### A. PMPC States

As in [8], [27], we account for the time-varying and unknown number of MPCs by introducing PMPCs indexed by  $k \in \{1, \dots, K_n\}$ . The number  $K_n$  of PMPCs is the maximum number of actual MPCs that have produced a measurement so far [27] (where  $K_n$  is increasing with time). The existence/nonexistence of PMPC  $k$  as an actual MPC is modeled by a binary random variable  $r_{k,n} \in \mathbb{S} = \{0, 1\}$  in the sense that a PMPC exists if and only if  $r_{k,n} = 1$ . Augmented states of PMPCs are denoted as  $\mathbf{y}_{k,n} \triangleq [\mathbf{x}_{k,n}^T \ r_{k,n}]^T \in \mathbb{R}^{5 \times 1} \times \mathbb{S}$ , where  $\mathbf{x}_{k,n} = [\theta_{k,n}^T \ \mathbf{u}_{k,n} \ \mathbf{v}_{dk,n} \ \mathbf{v}_{\varphi_{k,n}}]^T \in \mathbb{R}^{5 \times 1}$ ,  $\theta_{k,n} = [d_{k,n} \ \varphi_{k,n}]^T \in \mathbb{R}^{2 \times 1}$ , and  $\mathbf{v}_{dk,n}$  and  $\mathbf{v}_{\varphi_{k,n}}$  are the distance and angular velocities, respectively.

Formally, PMPC  $k$  is also considered if it is nonexistent, i.e.,  $r_{k,n} = 0$ . The states  $\mathbf{x}_{k,n}$  of nonexistent PMPCs are obviously irrelevant and have no influence on the PMPC detection and state estimation. Therefore, all PDFs defined for PMPC states,  $f(\mathbf{y}_{k,n}) = f(\mathbf{x}_{k,n}, r_{k,n})$ , are of the form  $f(\mathbf{x}_{k,n}, r_{k,n} = 0) = f_{k,n} f_D(\mathbf{x}_{k,n})$ , where  $f_D(\mathbf{x}_{k,n})$  is an arbitrary “dummy PDF” and  $f_{k,n} \in [0, 1]$  is a constant representing the probability of nonexistence [8], [27], [30].

#### B. State-Transition Model

For each PMPC with state  $\mathbf{y}_{k,n-1}$  with  $k \in \{1, \dots, K_{n-1}\}$  at time  $n-1$ , there is one “legacy” PMPC with state  $\underline{\mathbf{y}}_{k,n} \triangleq [\mathbf{x}_{k,n}^T \ r_{k,n}]^T$  with  $k \in \{1, \dots, K_{n-1}\}$  at time  $n$ . Assuming that PMPC states evolve independently across  $k$  and  $n$ , the according state-transition PDF of PMPC states  $\mathbf{y}_{n-1} \triangleq [\mathbf{y}_{1,n-1}^T \ \dots \ \mathbf{y}_{K_{n-1},n-1}^T]^T$  and legacy PMPC states  $\underline{\mathbf{y}}_n \triangleq [\underline{\mathbf{y}}_{1,n}^T \ \dots \ \underline{\mathbf{y}}_{K_{n-1},n}^T]^T$  factorizes as [8], [27]

$$f(\underline{\mathbf{y}}_n | \mathbf{y}_{n-1}) = \prod_{k=1}^{K_{n-1}} f(\underline{\mathbf{y}}_{k,n} | \mathbf{y}_{k,n-1}), \quad (3)$$

where  $f(\underline{\mathbf{y}}_{k,n} | \mathbf{y}_{k,n-1}) = f(\underline{\mathbf{x}}_{k,n}, \underline{r}_{k,n} | \mathbf{x}_{k,n-1}, r_{k,n-1})$  is the single PMPC state-transition PDF. If a PMPC did not exist at time  $n-1$ , i.e.,  $r_{k,n-1} = 0$ , it cannot exist at time  $n$  as a legacy PMPC. This means that

$$f(\underline{\mathbf{x}}_{k,n}, \underline{r}_{k,n} | \mathbf{x}_{k,n-1}, 0) = \begin{cases} f_D(\underline{\mathbf{x}}_{k,n}), & \underline{r}_{k,n} = 0 \\ 0, & \underline{r}_{k,n} = 1. \end{cases} \quad (4)$$

If a PMPC existed at time  $n-1$ , i.e.,  $r_{k,n-1} = 1$ , it either dies i.e.,  $\underline{r}_{k,n} = 0$  or it still exists i.e.,  $\underline{r}_{k,n} = 1$  with the survival probability denoted as  $p_s$ . If it does survive, the state  $\underline{\mathbf{x}}_{k,n}$  is distributed according to the state-transition PDF  $f(\underline{\mathbf{x}}_{k,n} | \mathbf{x}_{k,n-1})$ . Thus we have

$$f(\underline{\mathbf{x}}_{k,n}, \underline{r}_{k,n} | \mathbf{x}_{k,n-1}, 1) = \begin{cases} (1 - p_s)f_D(\underline{\mathbf{x}}_{k,n}), & \underline{r}_{k,n} = 0 \\ p_s f(\underline{\mathbf{x}}_{k,n} | \mathbf{x}_{k,n-1}), & \underline{r}_{k,n} = 1. \end{cases} \quad (5)$$

We also define the state vectors for all times up to  $n$  of legacy PMPCs as  $\underline{\mathbf{y}}_{1:n} \triangleq [\underline{\mathbf{y}}_1^T \cdots \underline{\mathbf{y}}_n^T]^T$ .

### C. Measurement Model

Before the current measurements  $\mathbf{z}_n$  are observed, the number of measurements  $M_n$  is a random variable. The vector collecting the number of measurements is defined as  $\mathbf{m}_{1:n} \triangleq [M_1 \cdots M_n]^T$ . The conditional PDF  $f(\mathbf{z}_{m,n} | \mathbf{x}_{k,n})$  of  $\mathbf{z}_n$  assumes that the individual measurements  $\mathbf{z}_{m,n}$  are conditionally independent given the state  $\mathbf{x}_{k,n}$ . (Details about the joint likelihood function are given in Appendix B.)

At each time  $n$ , a snapshot-based channel estimator provides the current observed measurement vector  $\mathbf{z}_n = [\mathbf{z}_{1,n}^T \cdots \mathbf{z}_{M_n,n}^T]^T$ , which is not random anymore and with fixed  $M_n$  (for details see for Section II). If  $\mathbf{z}_{m,n}$  is a *PMPC-oriented* measurement, we assume that the conditional PDF  $f(\mathbf{z}_{m,n} | \mathbf{x}_{k,n})$  is conditionally independent across  $\mathbf{z}_{d_{m,n}}$ ,  $\mathbf{z}_{\varphi_{m,n}}$ , and  $\mathbf{z}_{u_{m,n}}$  given the states  $\mathbf{d}_{k,n}$ ,  $\varphi_{k,n}$ , and  $\mathbf{u}_{k,n}$ , thus it factorizes as

$$f(\mathbf{z}_{m,n} | \mathbf{x}_{k,n}) = f(z_{d_{m,n}} | d_{k,n}, u_{k,n}) f(z_{\varphi_{m,n}} | \varphi_{k,n}, u_{k,n}) f(z_{u_{m,n}} | u_{k,n}) \quad (6)$$

where the individual likelihood functions of the distance measurement  $f(z_{d_{m,n}} | d_{k,n}, u_{k,n})$  and the AoA measurement  $f(z_{\varphi_{m,n}} | \varphi_{k,n}, u_{k,n})$  are modeled by Gaussian functions, i.e.,

$$f(z_{d_{m,n}} | d_{k,n}, u_{k,n}) = (2\pi\sigma_{d_{k,n}}^2)^{-\frac{1}{2}} e^{-\frac{(z_{d_{m,n}} - d_{k,n})^2}{2\sigma_{d_{k,n}}^2}} \quad (7)$$

and

$$f(z_{\varphi_{m,n}} | \varphi_{k,n}, u_{k,n}) = (2\pi\sigma_{\varphi_{k,n}}^2)^{-\frac{1}{2}} e^{\frac{-(z_{\varphi_{m,n}} - \varphi_{k,n})^2}{2\sigma_{\varphi_{k,n}}^2}}. \quad (8)$$

The variances depend on  $u_{k,n}$  and are determined based on the Fisher information given as  $\sigma_{d_{k,n}}^2 = c^2/(8\pi^2\beta_{bw}^2 u_{k,n}^2)$  and  $\sigma_{\varphi_{k,n}}^2 = c^2/(8\pi^2 f_c^2 u_{k,n}^2 D^2(\varphi_{k,n}))$  using the PMPC states by, respectively [33], [36]. Here,  $\beta_{bw}^2$  is the mean square bandwidth of the transmit signal pulse  $\tilde{s}(t)$  and  $D^2(\varphi_{k,n})$  is the squared array aperture. The likelihood function  $f(z_{u_{m,n}} | u_{k,n})$  of the normalized amplitude measurement  $z_{u_{m,n}}$  is modeled by a Rician function [26, Ch. 1.6.7], [32], [33], [37], i.e.,

$$f(z_{u_{m,n}} | u_{k,n}) = \frac{\frac{z_{u_{m,n}}}{\sigma_{u_{k,n}}^2} e^{\left(\frac{-(z_{u_{m,n}}^2 + u_{k,n}^2)}{2\sigma_{u_{k,n}}^2}\right)} I_0\left(\frac{z_{u_{m,n}} u_{k,n}}{\sigma_{u_{k,n}}^2}\right)}{p_d(u_{k,n})} \quad \text{for } z_{u_{m,n}} > u_{de} \quad (9)$$

where the spread parameter depends on  $u_{k,n}$  and is determined based on the Fisher information given as  $\sigma_{u_{k,n}}^2 = \frac{1}{2} + \frac{1}{4N_s H} u_{k,n}^2$ , and  $I_0(\cdot)$  represents the 0th order modified first-kind Bessel function. (Details about the derivation of the variance  $\sigma_{u_{k,n}}^2$  are given in Appendix D.) The detection probability (i.e., the probability that a PMPC  $\mathbf{y}_{k,n}$  generates a measurement  $z_{m,n}$ ) is modeled by a Rician cumulative distribution function (CDF), i.e.,  $p_d(u_{k,n}) = Q_1(u_{k,n}/\sigma_{u_{k,n}}, u_{de}/\sigma_{u_{k,n}})$  [31]–[33], where the CDF  $Q_1(\cdot, \cdot)$  denotes the Marcum Q-function [26, Ch. 1.6.7] and  $u_{de}$  the preprocessing-related detection threshold. Note that  $p_d(u_{k,n})$  is directly related to the MPC’s visibility and the component SNR as well as the preprocessing-related detection threshold  $u_{de}$  of the snapshot-based channel estimator.

False alarm measurements are assumed statistically independent of PMPC states. They are modeled by a Poisson point process with mean  $\mu_{fa,n}$  and PDFs  $f_{fa}(z_{m,n})$ , which factorize as  $f_{fa}(z_{m,n}) = f_{fad}(z_{dm,n}) f_{fa\varphi}(z_{\varphi_{m,n}}) f_{fa_u}(z_{u_{m,n}})$ , where  $f_{fad}(z_{dm,n})$  and  $f_{fa\varphi}(z_{\varphi_{m,n}})$  are assumed to be uniform, i.e.,  $f_{fad}(z_{dm,n}) = 1/d_{\max}$  and  $f_{fa\varphi}(z_{\varphi_{m,n}}) = 1/2\pi$ . With noise only, the Rician distribution in (9) degenerates to a Rayleigh distribution, thus the false alarm PDF  $f_{fa_u}(z_{u_{m,n}})$  of the normalized amplitude is given as  $f_{fa_u}(z_{u_{m,n}}) = 2z_{u_{m,n}} \exp(-z_{u_{m,n}}^2)/p_{fa}$  for  $z_{u_{m,n}} > u_{de}$  where  $p_{fa} = \exp(-u_{de}^2)$  denotes the false alarm probability [26, Ch. 1.6.7]. The amplitude model discrimination is further exploited for probabilistic DA in the form of likelihood ratio in the pseudo likelihood functions (15) and (16).

The mean FAR  $\mu_{fa,n}$  is assumed unknown, time-varying, and automatically adapted online in the proposed algorithm. It evolves across time according to the state-transition PDF  $f(\mu_{fa,n} | \mu_{fa,n-1})$ .

The state vector for all times up to  $n$  is given as  $\boldsymbol{\mu}_{\text{fa},1:n} \triangleq [\mu_{\text{fa},1} \cdots \mu_{\text{fa},n}]^T$ .

#### D. New PMPCs

Newly detected PMPCs, i.e., PMPCs that generated measurements for the first time, are modeled by a Poisson point process with mean  $\mu_n$  and PDF  $f_n(\bar{\mathbf{x}}_{m,n})$ . Following [8], [27], newly detected PMPCs are represented by new PMPC states  $\bar{\mathbf{y}}_{m,n} \triangleq [\bar{\mathbf{x}}_{m,n}^T \bar{r}_{m,n}]^T$ ,  $m \in \{1, \dots, M_n\}$ . Each new PMPC  $\bar{\mathbf{y}}_{m,n}$  corresponds to a measurement  $\mathbf{z}_{m,n}$ , thus the number of new PMPCs at time  $n$  equals to the number of measurements  $M_n$ . Here,  $\bar{r}_{m,n} = 1$  means that the measurement  $\mathbf{z}_{m,n}$  was generated by a newly detected PMPC. The state vector of all new PMPCs at time  $n$  is given by  $\bar{\mathbf{y}}_n \triangleq [\bar{\mathbf{y}}_{1,n}^T \cdots \bar{\mathbf{y}}_{M_n,n}^T]^T$  and state vector for all times up to  $n$  by  $\bar{\mathbf{y}}_{1:n} \triangleq [\bar{\mathbf{y}}_1^T \cdots \bar{\mathbf{y}}_n^T]^T$ . The new PMPCs become legacy PMPCs when the measurements at next time are observed, accordingly the number of legacy PMPCs is updated as  $K_n = K_{n-1} + M_n$ . The vector containing all PMPC states at time  $n$  is given by  $\mathbf{y}_n \triangleq [\mathbf{y}_n^T \bar{\mathbf{y}}_n^T]^T$ , where  $\mathbf{y}_{k,n}$  with  $k \in \{1, \dots, K_n\}$ , and state vector for all times up to  $n$  by  $\mathbf{y}_{1:n} \triangleq [\mathbf{y}_1^T \cdots \mathbf{y}_n^T]^T$ .

#### E. Data Association Uncertainty

Estimation of multiple MPCs states is complicated by the DA uncertainty, i.e., it is unknown which measurement  $\mathbf{z}_{m,n}$  originated from which MPC. Furthermore, it is not known if a measurement did not originate from a PMPC (false alarm), or if a PMPC did not generate any measurement (missed detection). Following [8], [27], the unknown DA are described by the *PMPC-oriented* association vector  $\mathbf{a}_n \triangleq [a_{1,n} \cdots a_{K_{n-1},n}]^T$  with entries

$$a_{k,n} \triangleq \begin{cases} m \in \{1, \dots, M_n\}, & \text{if legacy PMPC } k \text{ generates measurement } m \\ 0, & \text{if legacy PMPC } k \text{ does not generate any measurement} \end{cases} \quad (10)$$

or equivalently by the *measurement-oriented* association vector  $\mathbf{b}_n \triangleq [b_{1,n} \cdots b_{M_n,n}]^T$  as presented in [8], [27], [38], with entries

$$b_{m,n} \triangleq \begin{cases} k \in \{1, \dots, K_{n-1}\}, & \text{if measurement } m \text{ is generated by legacy PMPC } k \\ 0, & \text{if measurement } m \text{ is not generated by any legacy PMPC.} \end{cases} \quad (11)$$

Here, we follow the assumption that at each time  $n$  a PMPC can generate at most one measurement, namely that a measurement can be generated by at most one PMPC, either a legacy or

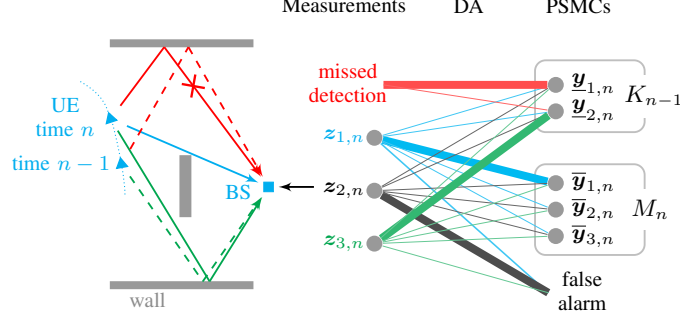


Fig. 1: An example of probabilistic DA, where the association probability from a measurement to a PMPC is proportional to the line thickness. At time  $n$ , three measurements are generated from the snapshot-based estimator. The probability that the measurement  $z_{1,n}$  (originated from the emerging LoS path) is associated with the new PMPC state  $\bar{y}_{1,n}$  is much higher than the probability that  $z_{1,n}$  is associated with a legacy PMPC. The measurement  $z_{3,n}$  (originated from the 1st order reflection MPC) is associated with the legacy PMPC state  $y_{2,n}$  with high probability. Besides, it is highly possible that the measurement  $z_{2,n}$  is a false alarm and the legacy PMPC state  $y_{1,n}$  did not generate any measurement (missed detection).

a new one. This is enforced by the exclusion functions  $\Psi(\mathbf{a}_n, \mathbf{b}_n)$  and  $\Gamma_{\mathbf{a}_n}(\bar{r}_{m,n})$ . The function  $\Psi(\mathbf{a}_n, \mathbf{b}_n) = \prod_{k=1}^{K_{n-1}} \prod_{m=1}^{M_n} \psi(a_{k,n}, b_{m,n})$  [8], [27], [38] is defined as

$$\psi(a_{k,n}, b_{m,n}) = \begin{cases} 0, & a_{k,n} = m, b_{m,n} \neq k \text{ or } b_{m,n} = k, a_{k,n} \neq m \\ 1, & \text{otherwise} \end{cases} \quad (12)$$

and the function  $\Gamma_{\mathbf{a}_n}(\bar{r}_{m,n}) = 0$  if  $\bar{r}_{m,n} = 1$  and  $a_{k,n} = m$ , otherwise it equals 1. (Details can be found in Appendix A.) The “redundant formulation” of using  $\mathbf{a}_n$  together with  $\mathbf{b}_n$  is the key to make the algorithm scalable to the varying numbers of PMPCs and measurements. The association vectors for all times up to  $n$  are given by  $\mathbf{a}_{1:n} \triangleq [\mathbf{a}_1^T \cdots \mathbf{a}_n^T]^T$  and  $\mathbf{b}_{1:n} \triangleq [\mathbf{b}_1^T \cdots \mathbf{b}_n^T]^T$ , respectively.

Fig. 1 conceptually illustrates the DA between measurements and PMPC states. The probabilities of all association hypotheses of PMPCs and measurements are evaluated, and a high probability indicates that the PMPC state explains a measurement well. After computing the DA probabilities, the PMPC states are updated by considering all the measurements.

#### IV. JOINT POSTERIOR PDF AND PROBLEM FORMULATION

##### A. The Joint Posterior PDF and the Factor Graph

By using the common assumptions [8], [26], [27], and fixed and thus observed measurements  $\mathbf{z}_{1:n}$ , the joint posterior PDF of  $\mathbf{y}_{1:n}$ ,  $\mathbf{a}_{1:n}$ ,  $\mathbf{b}_{1:n}$ ,  $\mathbf{m}_{\text{fa},1:n}$ , and  $\mathbf{m}_{1:n}$  conditioned on the observed

measurement vector  $\mathbf{z}_{1:n}$  is given as

$$\begin{aligned}
& f(\mathbf{y}_{1:n}, \mathbf{a}_{1:n}, \mathbf{b}_{1:n}, \boldsymbol{\mu}_{\text{fa},1:n}, \mathbf{m}_{1:n} | \mathbf{z}_{1:n}) \\
&= f(\underline{\mathbf{y}}_{1:n}, \bar{\mathbf{y}}_{1:n}, \mathbf{a}_{1:n}, \mathbf{b}_{1:n}, \boldsymbol{\mu}_{\text{fa},1:n}, \mathbf{m}_{1:n} | \mathbf{z}_{1:n}) \\
&\propto f(\mathbf{z}_{1:n} | \underline{\mathbf{y}}_{1:n}, \bar{\mathbf{y}}_{1:n}, \mathbf{a}_{1:n}, \mathbf{b}_{1:n}, \mathbf{m}_{1:n}) f(\underline{\mathbf{y}}_{1:n}, \bar{\mathbf{y}}_{1:n}, \mathbf{a}_{1:n}, \mathbf{b}_{1:n}, \boldsymbol{\mu}_{\text{fa},1:n}, \mathbf{m}_{1:n}).
\end{aligned} \tag{13}$$

After inserting the expressions (43) and (49) and performing some simple manipulations, the joint posterior PDF in (13) can be rewritten as

$$\begin{aligned}
& f(\underline{\mathbf{y}}_{1:n}, \bar{\mathbf{y}}_{1:n}, \mathbf{a}_{1:n}, \mathbf{b}_{1:n}, \boldsymbol{\mu}_{\text{fa},1:n}, \mathbf{m}_{1:n} | \mathbf{z}_{1:n}) \\
&\propto f(\boldsymbol{\mu}_{\text{fa},1}) \prod_{l=1}^{M_1} h(\bar{\mathbf{y}}_{l,1}, b_{l,1}, \boldsymbol{\mu}_{\text{fa},1}; \mathbf{z}_1) \prod_{n'=2}^n f(\boldsymbol{\mu}_{\text{fa},n'} | \boldsymbol{\mu}_{\text{fa},n'-1}) \left( \prod_{k'=1}^{K_{n'-1}} f(\underline{\mathbf{y}}_{k',n'} | \mathbf{y}_{k',n'-1}) \right) \\
&\times \left( \prod_{k=1}^{K_{n'-1}} g(\underline{\mathbf{y}}_{k,n'}, a_{k,n'}, \boldsymbol{\mu}_{\text{fa},n'}; \mathbf{z}_{n'}) \prod_{m=1}^{M_{n'}} \psi(a_{k,n'}, b_{m,n'}) \right) \left( \prod_{m'=1}^{M_{n'}} h(\bar{\mathbf{y}}_{m',n'}, b_{m',n'}, \boldsymbol{\mu}_{\text{fa},n'}; \mathbf{z}_{n'}) \right)
\end{aligned} \tag{14}$$

where the functions  $g(\underline{\mathbf{y}}_{k,n}, a_{k,n}, \boldsymbol{\mu}_{\text{fa},n}; \mathbf{z}_n)$  and  $h(\bar{\mathbf{y}}_{m,n}, b_{m,n}, \boldsymbol{\mu}_{\text{fa},n}; \mathbf{z}_n)$  will be discussed next.

The *pseudo likelihood functions*  $g(\underline{\mathbf{y}}_{k,n}, a_{k,n}, \boldsymbol{\mu}_{\text{fa},n}; \mathbf{z}_n) = g(\underline{\mathbf{x}}_{k,n}, \underline{r}_{k,n}, a_{k,n}, \boldsymbol{\mu}_{\text{fa},n}; \mathbf{z}_n)$  and  $h(\bar{\mathbf{y}}_{m,n}, b_{m,n}, \boldsymbol{\mu}_{\text{fa},n}; \mathbf{z}_n) = h(\bar{\mathbf{x}}_{m,n}, \bar{r}_{m,n}, b_{m,n}, \boldsymbol{\mu}_{\text{fa},n}; \mathbf{z}_n)$  are given by

$$g(\underline{\mathbf{x}}_{k,n}, \underline{r}_{n,k} = 1, a_{k,n}, \boldsymbol{\mu}_{\text{fa},n}; \mathbf{z}_n) = \begin{cases} \frac{n(\boldsymbol{\mu}_{\text{fa},n}) f(\mathbf{z}_{m,n} | \underline{\mathbf{x}}_{k,n}) p_d(u_{k,n})}{\boldsymbol{\mu}_{\text{fa},n} f_{\text{fa}}(\mathbf{z}_{m,n})}, & a_{k,n} = m \\ 1 - p_d(u_{k,n}), & a_{k,n} = 0 \end{cases} \tag{15}$$

and  $g(\underline{\mathbf{x}}_{k,n}, \underline{r}_{n,k} = 0, a_{k,n}, \boldsymbol{\mu}_{\text{fa},n}; \mathbf{z}_n) = \bar{1}(a_{k,n}) n(\boldsymbol{\mu}_{\text{fa},n})$  with a factor related to mean FAR  $n(\boldsymbol{\mu}_{\text{fa},n}) \triangleq (\boldsymbol{\mu}_{\text{fa},n}^{M_n} e^{-\boldsymbol{\mu}_{\text{fa},n}} / M_n!)^{1/(K_{n-1} + M_n)}$  and by

$$h(\bar{\mathbf{x}}_{m,n}, \bar{r}_{m,n} = 1, b_{m,n}, \boldsymbol{\mu}_{\text{fa},n}; \mathbf{z}_n) = \begin{cases} 0, & b_{m,n} = k \\ \frac{n(\boldsymbol{\mu}_{\text{fa},n}) \mu_n f_n(\bar{\mathbf{x}}_{m,n}) f(\mathbf{z}_{m,n} | \bar{\mathbf{x}}_{m,n})}{\boldsymbol{\mu}_{\text{fa},n} f_{\text{fa}}(\mathbf{z}_{m,n})}, & b_{m,n} = 0 \end{cases} \tag{16}$$

and  $h(\bar{\mathbf{x}}_{m,n}, \bar{r}_{m,n} = 0, b_{m,n}, \boldsymbol{\mu}_{\text{fa},n}; \mathbf{z}_n) = n(\boldsymbol{\mu}_{\text{fa},n})$ , respectively. The factor graph [39], [40] representing the factorization in (14) is shown in Fig. 2. A detailed derivation of the joint posterior PDF in (14) is provided in the Appendix in Section A, Section B, and Section C.

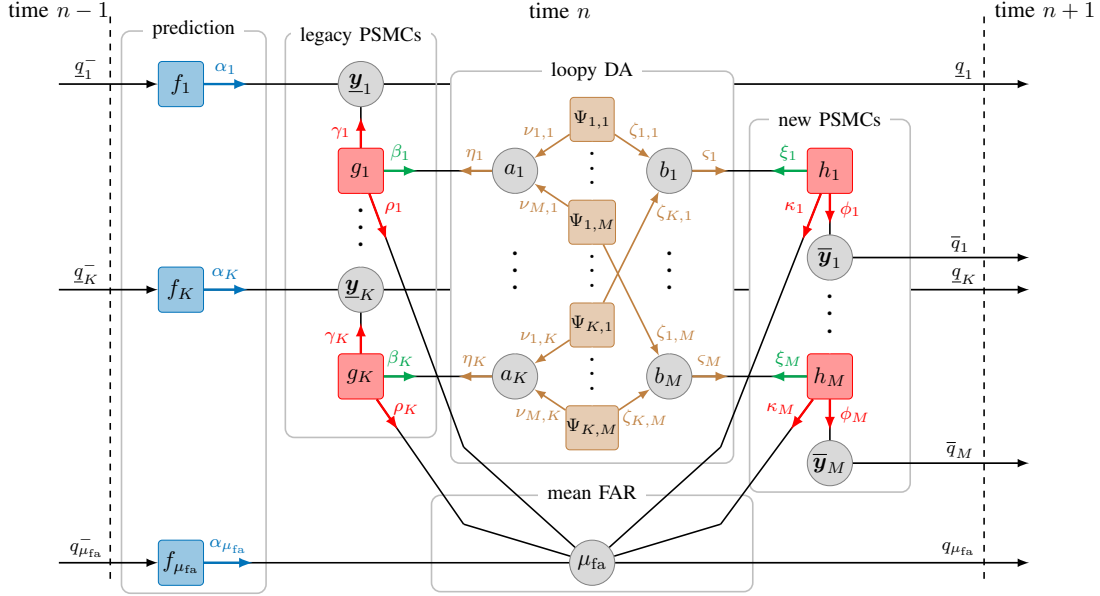


Fig. 2: Factor graph representation of the factorized joint posterior PDF (14), shown for time  $n$ . For simplicity, the following short notations are used:  $K \triangleq K_{n-1}$ ,  $M \triangleq M_n$ ; variable nodes:  $a_k \triangleq a_{k,n}$ ,  $b_m \triangleq b_{m,n}$ ,  $\mu_{\text{fa}} \triangleq \mu_{\text{fa},n}$ ,  $\underline{y}_k \triangleq \underline{y}_{k,n}$ ,  $\bar{y}_m \triangleq \bar{y}_{m,n}$ ; factor nodes:  $f_k \triangleq f(\underline{y}_{k,n} | \underline{y}_{k,n-1})$ ,  $f_{\mu_{\text{fa}}} \triangleq f(\mu_{\text{fa},n} | \mu_{\text{fa},n-1})$ ,  $g_k \triangleq g(\underline{x}_{k,n}, \underline{r}_{k,n}, a_{k,n}, \mu_{\text{fa},n}; \underline{z}_n)$ ,  $h_m \triangleq h(\bar{x}_{m,n}, \bar{r}_{m,n}, b_{m,n}, \mu_{\text{fa},n}; \underline{z}_n)$ ,  $\Psi_{k,m} \triangleq \Psi(a_{k,n}, b_{m,n})$ ; prediction:  $\alpha_k \triangleq \alpha(\underline{x}_{k,n}, \underline{r}_{k,n})$ ,  $\alpha_{\mu_{\text{fa}}} \triangleq \alpha(\mu_{\text{fa},n})$ ; measurement evaluation:  $\beta_k \triangleq \beta(a_k)$ ,  $\xi_m \triangleq \xi(b_m)$ ; loopy DA:  $\nu_{m,k} \triangleq \nu_{m \rightarrow k}(a_{k,n})$ ,  $\zeta_{k,m} \triangleq \zeta_{k \rightarrow m}(b_{m,n})$ ,  $\eta_k \triangleq \eta(a_k)$ ,  $\varsigma_m \triangleq \varsigma(b_m)$ ; measurement update:  $\gamma_k \triangleq \gamma(\underline{x}_{k,n}, \underline{r}_{k,n})$ ,  $\rho_k \triangleq \rho_k(\mu_{\text{fa},n})$ ,  $\phi_m \triangleq \phi(\bar{x}_{m,n}, \bar{r}_{m,n})$ ,  $\kappa_m \triangleq \kappa_m(\mu_{\text{fa},n})$ ; belief calculation:  $\underline{q}_k \triangleq q(\underline{x}_{k,n-1}, \underline{r}_{k,n-1})$ ,  $\underline{q}_k \triangleq q(\underline{x}_{k,n}, \underline{r}_{k,n})$ ,  $\bar{q}_m \triangleq \bar{q}(\bar{x}_{m,n}, \bar{r}_{m,n})$ ,  $q_{\mu_{\text{fa}}}^- \triangleq q(\mu_{\text{fa},n-1})$ ,  $q_{\mu_{\text{fa}}} \triangleq q(\mu_{\text{fa},n})$ .

### B. PMPC Detection and State Estimation

The problem considered is the PMPCs' sequential detection and estimation of their states  $\underline{y}_{k,n}$ ,  $k \in \{1, \dots, K_{n-1} + M_n\}$  along with the estimation of mean FAR  $\mu_{\text{fa},n}$  from the observed measurement vector  $\underline{z}_{1:n} \triangleq [\underline{z}_1^T, \dots, \underline{z}_n^T]^T$  for all times up to  $n$ . This relies on the marginal posterior existence probabilities  $p(r_{k,n} = 1 | \underline{z}_{1:n})$ , the marginal posterior PDFs  $f(\underline{x}_{k,n} | r_{k,n} = 1, \underline{z}_{1:n})$  and  $f(\mu_{\text{fa},n} | \underline{z})$ . More specifically, a PMPC is detected if  $p(r_{k,n} = 1 | \underline{z}_{1:n}) > p_{\text{de}}$  [41]. To avoid confusion, in what follows  $p_{\text{de}}$  is termed as the existence probability threshold and  $u_{\text{de}}$  the preprocessing-related detection threshold. The probabilities  $p(r_{k,n} = 1 | \underline{z}_{1:n})$  are obtained from the marginal posterior PDFs of the PMPC states,  $f(\underline{y}_{k,n} | \underline{z}_{1:n}) = f(\underline{x}_{k,n}, r_{k,n} | \underline{z}_{1:n})$ , according to

$$p(r_{k,n} = 1 | \underline{z}_{1:n}) = \langle f(\underline{x}_{k,n}, r_{k,n} = 1 | \underline{z}_{1:n}) \rangle_{1_{\mathbb{R}^{5 \times 1}(\underline{x}_{k,n})}} \quad (17)$$

and the marginal posterior PDFs  $f(\mathbf{x}_{k,n}|r_{k,n} = 1, \mathbf{z}_{1:n})$  can be obtained from  $f(\mathbf{x}_{k,n}, r_{k,n}|\mathbf{z}_{1:n})$  as

$$f(\mathbf{x}_{k,n}|r_{k,n} = 1, \mathbf{z}_{1:n}) = \frac{f(\mathbf{x}_{k,n}, r_{k,n} = 1|\mathbf{z}_{1:n})}{p(r_{k,n} = 1|\mathbf{z}_{1:n})}. \quad (18)$$

The number of detected PMPCs represents an estimate of the number of MPCs given by  $\hat{L}_n$ . The states  $\mathbf{u}_{k,n}$  and  $\boldsymbol{\theta}_{k,n}$  of detected PMPCs are estimated by means of the minimum mean-square error (MMSE) estimator [42], i.e.,

$$u_{k,n}^{\text{MMSE}} \triangleq \langle u_{k,n} \rangle_{f(\mathbf{x}_{k,n}|r_{k,n}=1, \mathbf{z}_{1:n})}, \quad (19)$$

$$\boldsymbol{\theta}_{k,n}^{\text{MMSE}} \triangleq \langle \boldsymbol{\theta}_{k,n} \rangle_{f(\mathbf{x}_{k,n}|r_{k,n}=1, \mathbf{z}_{1:n})} \quad (20)$$

with  $\boldsymbol{\theta}_{k,n}^{\text{MMSE}} = [d_{k,n}^{\text{MMSE}} \varphi_{k,n}^{\text{MMSE}}]^T \in \mathbb{R}^{2 \times 1}$ , respectively. Note that the estimated component SNRs is given by  $\text{SNR}_{k,n}^{\text{MMSE}} = (u_{k,n}^{\text{MMSE}})^2$ . Finally, the estimate of the mean FAR  $\mu_{\text{fa},n}$  is given by

$$\mu_{\text{fa},n}^{\text{MMSE}} \triangleq \langle \mu_{\text{fa},n} \rangle_{f(\mu_{\text{fa},n}|\mathbf{z}_{1:n})}. \quad (21)$$

To avoid that the number of PMPCs grows indefinitely (at each time the number grows according to  $K_n = K_{n-1} + M_n$ ), PMPCs with  $p(r_{k,n} = 1|\mathbf{z}_{1:n})$  below a threshold  $p_{\text{pr}}$  are removed from the state space (“pruned”). For initialization of the snapshot-based channel estimator we also define  $\sigma_{d_{k,n}}^{\text{MMSE}} = (\langle (d_{k,n} - d_{k,n}^{\text{MMSE}})^2 \rangle_{f(\mathbf{x}_{k,n}|r_{k,n}=1, \mathbf{z}_{1:n})})^{\frac{1}{2}}$  and  $\sigma_{\varphi_{k,n}}^{\text{MMSE}} = (\langle (\varphi_{k,n} - \varphi_{k,n}^{\text{MMSE}})^2 \rangle_{f(\mathbf{x}_{k,n}|r_{k,n}=1, \mathbf{z}_{1:n})})^{\frac{1}{2}}$  (see for Section II-B).

## V. THE BP-MPC-SDE ALGORITHM

The posterior PDFs  $f(\underline{\mathbf{x}}_{k,n}, \underline{r}_{k,n}|\mathbf{z}_{1:n})$ ,  $f(\bar{\mathbf{x}}_{m,n}, \bar{r}_{m,n}|\mathbf{z}_{1:n})$ , and  $f(\mu_{\text{fa},n}|\mathbf{z}_{1:n})$  involved in (21)-(20) are marginal PDFs of the joint posterior PDF  $f(\mathbf{y}_{1:n}, \mathbf{a}_{1:n}, \mathbf{b}_{1:n}, \boldsymbol{\mu}_{\text{fa},1:n}, \mathbf{m}_{1:n}|\mathbf{z}_{1:n})$ . Since direct marginalization of the joint posterior PDF is infeasible, we use loopy (iterative) BP [39] by means of the SPA rules [39], [40] on the factor graph shown in Fig. 2. Due to the loops inside the factor graph, the resulting beliefs  $\underline{q}(\underline{\mathbf{y}}_{k,n}) = \underline{q}(\underline{\mathbf{x}}_{k,n}, \underline{r}_{k,n})$ ,  $\bar{q}(\bar{\mathbf{y}}_{m,n}) = \bar{q}(\bar{\mathbf{x}}_{m,n}, \bar{r}_{m,n})$ , and  $q(\mu_{\text{fa},n})$  are only approximations of the respective posterior marginal PDFs, and there is no canonical order in which the messages should be computed [39]. For the proposed algorithm, we specify the following order in which the message are computed: (i) messages are not sent backward in time; (ii) iterative message passing is only performed for probabilistic DA at each time  $n$ . Combining the specified order with the generic BP rules for calculating messages and

beliefs yields the following calculations at each time  $n$  (which are in parts in line with [8], [27, Ch. III]):

- 1) *Prediction*: First, a prediction step is performed. The prediction for the mean FAR state  $\mu_{fa,n}$  given by

$$\alpha(\mu_{fa,n}) = \langle f(\mu_{fa,n} | \mu_{fa,n-1}) \rangle_{q(\mu_{fa,n-1})} \quad (22)$$

and for all the legacy PMPCs given by

$$\alpha(\underline{x}_{k,n}, \underline{r}_{k,n}) = \sum_{r_{k,n-1} \in \{0,1\}} \langle f(\underline{x}_{k,n}, \underline{r}_{k,n} | \underline{x}_{k,n-1}, r_{k,n-1}) \rangle_{\underline{q}(\underline{x}_{k,n-1}, r_{k,n-1})}, \quad (23)$$

where  $q(\mu_{fa,n-1})$  and  $\underline{q}(\underline{x}_{k,n-1}, r_{k,n-1})$  were calculated at the previous time  $n-1$ . After substituting the PMPC state-transition PDFs in (23) with (4) and (5) respectively, we obtain the prediction message for legacy PMPCs as

$$\alpha(\underline{x}_{k,n}, 1) = p_s \langle f(\underline{x}_{k,n} | \underline{x}_{k,n-1}) \rangle_{\underline{q}(\underline{x}_{k,n-1}, 1)} \quad (24)$$

and  $\alpha(\underline{x}_{k,n}, 0) = \alpha_{k,n} f_D(\underline{x}_{k,n})$  with

$$\alpha_{k,n} = (1 - p_s) \langle \underline{q}(\underline{x}_{k,n-1}, 1) \rangle_{1_{\mathbb{R}^{5 \times 1}}(\underline{x}_{k,n-1})} + \underline{q}_{k,n-1}, \quad (25)$$

where  $\alpha_{k,n} \triangleq \langle \alpha(\underline{x}_{k,n}, 0) \rangle_{1_{\mathbb{R}^{5 \times 1}}(\underline{x}_{k,n})}$  and  $\underline{q}_{k,n-1} \triangleq \langle \underline{q}(\underline{x}_{k,n-1}, 0) \rangle_{1_{\mathbb{R}^{5 \times 1}}(\underline{x}_{k,n-1})}$ . After the prediction step, the following steps are performed for all legacy and new PMPCs in parallel:

- 2) *Measurement evaluation*: For legacy PMPCs, the messages  $\beta(a_{k,n})$  passed from the factor nodes  $g(\underline{x}_{k,n}, \underline{r}_{k,n}, a_{k,n}, \mu_{fa,n}; \underline{z}_n)$  to the PMPC-oriented DA variable nodes  $a_{k,n}$  are calculated by

$$\begin{aligned} \beta(a_{k,n}) &= \langle \langle g(\underline{x}_{k,n}, 1, a_{k,n}, \mu_{fa,n}; \underline{z}_n) \rangle_{\alpha(\underline{x}_{k,n}, 1)} \rangle_{\alpha(\mu_{fa,n})} \\ &\quad + \bar{1}(a_{k,n}) \langle \langle \alpha(\underline{x}_{k,n}, 0) n(\mu_{fa,n}) \rangle_{1_{\mathbb{R}^{5 \times 1}}(\underline{x}_{k,n})} \rangle_{\alpha(\mu_{fa,n})}. \end{aligned} \quad (26)$$

For new PMPCs, the messages  $\xi(b_{m,n})$  passed from the factor nodes  $h(\bar{\underline{x}}_{m,n}, \bar{\underline{r}}_{m,n}, b_{m,n}, \mu_{fa,n}; \underline{z}_n)$  to the measurement-oriented DA variable nodes  $b_{m,n}$  are calculated according to

$$\xi(b_{m,n}) = \sum_{\bar{r}_{m,n} \in \{0,1\}} \langle \langle h(\bar{\underline{x}}_{m,n}, \bar{\underline{r}}_{m,n}, b_{m,n}, \mu_{fa,n}; \underline{z}_n) \rangle_{1_{\mathbb{R}^{5 \times 1}}(\bar{\underline{x}}_{m,n})} \rangle_{\alpha(\mu_{fa,n})}. \quad (27)$$

More specifically, for  $b_{m,n} = k$  it becomes

$$\xi(b_{m,n}) = \langle n(\mu_{fa,n}) \alpha(\mu_{fa,n}) \rangle_{1_{\mathbb{R}}(\mu_{fa,n})} \quad (28)$$

and for  $b_{m,n} = 0$  it becomes

$$\begin{aligned}\xi(b_{m,n}) &= \langle n(\mu_{fa,n}) \alpha(\mu_{fa,n}) \rangle_{1_{\mathbb{R}}(\mu_{fa,n})} \\ &+ \left\langle \left\langle \frac{\mu_n f_n(\bar{\mathbf{x}}_{m,n}) n(\mu_{fa,n}) f(\mathbf{z}_{m,n} | \bar{\mathbf{x}}_{m,n})}{\mu_{fa,n} f_{fa}(\mathbf{z}_{m,n})} \right\rangle_{1_{\mathbb{R}^{5 \times 1}}(\bar{\mathbf{x}}_{m,n})} \right\rangle_{\alpha(\mu_{fa,n})}.\end{aligned}\quad (29)$$

3) *Iterative probabilistic DA*: With the messages  $\beta(a_{k,n})$  and  $\xi(b_{m,n})$ , the probabilistic DA messages  $\eta(a_{k,n})$  and  $\varsigma(b_{m,n})$  are obtained with an efficient loopy BP algorithm as shown in [8], [30], [38]

$$\eta(a_{k,n}) = \prod_{m=1}^{M_n} \nu_{\psi_{m \rightarrow k}}^{(p)}(a_{k,n}) \quad \text{and} \quad \varsigma(b_{m,n}) = \prod_{k=1}^{K_{n-1}} \zeta_{\psi_{k \rightarrow m}}^{(p)}(b_{m,n}) \quad (30)$$

where  $\nu_{\psi_{m \rightarrow k}}^{(p)}(a_{k,n})$  and  $\zeta_{\psi_{k \rightarrow m}}^{(p)}(b_{m,n})$  denote the messages passed from  $\psi(a_{k,n}, b_{m,n})$  to the variable node  $a_{k,n}$  and  $b_{m,n}$  at each iteration  $p \in \{1, \dots, P\}$ , respectively.

4) *Measurement update*: For legacy PMPCs, the messages  $\gamma(\underline{\mathbf{x}}_{k,n}, \underline{r}_{k,n})$  passed from the factor nodes  $g(\underline{\mathbf{x}}_{k,n}, \underline{r}_{k,n}, a_{k,n}, \mu_{fa,n}; \mathbf{z}_n)$  to the variable nodes  $\underline{\mathbf{y}}_{k,n}$  are calculated by

$$\gamma(\underline{\mathbf{x}}_{k,n}, 1) = \sum_{a_{k,n}=0}^{M_n} \eta(a_{k,n}) \langle g(\underline{\mathbf{x}}_{k,n}, 1, a_{k,n}, \mu_{fa,n}; \mathbf{z}_n) \rangle_{\alpha(\mu_{fa,n})} \quad (31)$$

and  $\gamma(\underline{\mathbf{x}}_{k,n}, 0) = \gamma_{k,n} f_D(\underline{\mathbf{x}}_{k,n})$  with

$$\gamma_{k,n} = \langle \gamma(\underline{\mathbf{x}}_{k,n}, 0) \rangle_{1_{\mathbb{R}^{5 \times 1}}(\underline{\mathbf{x}}_{k,n})} = \eta(0) \langle n(\mu_{fa,n}) \rangle_{\alpha(\mu_{fa,n})}. \quad (32)$$

For new PMPCs, the messages  $\phi(\bar{\mathbf{x}}_{m,n}, \bar{r}_{m,n})$  passed from the factor nodes  $h(\bar{\mathbf{x}}_{m,n}, \bar{r}_{m,n}, b_{m,n}, \mu_{fa,n}; \mathbf{z}_n)$  to the variable nodes  $\bar{\mathbf{y}}_{m,n}$  are calculated by

$$\phi(\bar{\mathbf{x}}_{m,n}, 1) = \varsigma(0) \langle h(\bar{\mathbf{x}}_{m,n}, 1, b_{m,n}, \mu_{fa,n}; \mathbf{z}_n) \rangle_{\alpha(\mu_{fa,n})} \quad (33)$$

and  $\phi(\bar{\mathbf{x}}_{m,n}, 0) = \phi_{m,n} f_D(\bar{\mathbf{x}}_{m,n})$  with

$$\phi_{m,n} \triangleq \langle \phi(\bar{\mathbf{x}}_{m,n}, 0) \rangle_{1_{\mathbb{R}^{5 \times 1}}(\bar{\mathbf{x}}_{m,n})} = \sum_{b_{m,n}=0}^{K_{n-1}} \varsigma(b_{m,n}) \langle n(\mu_{fa,n}) \rangle_{\alpha(\mu_{fa,n})}. \quad (34)$$

For the mean FAR  $\mu_{fa,n}$ , the messages  $\rho_k(\mu_{fa,n})$  and  $\kappa_m(\mu_{fa,n})$  passed from the factor nodes  $g(\underline{\mathbf{x}}_{k,n}, \underline{r}_{k,n}, a_{k,n}, \mu_{fa,n}; \mathbf{z}_n)$  and  $h(\bar{\mathbf{x}}_{m,n}, \bar{r}_{m,n}, b_{m,n}, \mu_{fa,n}; \mathbf{z}_n)$ , respectively, to the variable

node  $\mu_{\text{fa},n}$  are calculated by

$$\rho_k(\mu_{\text{fa},n}) = \sum_{a_{k,n}=0}^{M_n} \eta(a_{k,n}) \sum_{\underline{r}_{k,n} \in \{0,1\}} \langle g(\underline{\mathbf{x}}_{k,n}, \underline{r}_{k,n}, a_{k,n}, \mu_{\text{fa},n}; \mathbf{z}_n) \rangle_{\alpha(\underline{\mathbf{x}}_{k,n}, \underline{r}_{k,n})} \quad (35)$$

and

$$\kappa_m(\mu_{\text{fa},n}) = n(\mu_{\text{fa},n}) \varsigma(0) \left\langle \frac{\mu_{\text{n}} f(\mathbf{z}_{m,n} | \bar{\mathbf{x}}_{m,n})}{\mu_{\text{fa},n} f_{\text{fa}}(\mathbf{z}_{m,n})} \right\rangle_{f_{\text{n}}(\bar{\mathbf{x}}_{m,n})} + \sum_{b_{m,n}=0}^{K_{n-1}} \varsigma(b_{m,n}) n(\mu_{\text{fa},n}). \quad (36)$$

5) *Belief calculation:* With all the messages above, the approximations of the marginal posterior PDFs needed for the MMSE estimations in Section IV-B are calculated as follows. The beliefs  $\underline{q}(\underline{\mathbf{y}}_{k,n}) = \underline{q}(\underline{\mathbf{x}}_{k,n}, \underline{r}_{k,n})$  approximating the marginal posterior PDFs  $f(\underline{\mathbf{y}}_{k,n} | \mathbf{z}_{1:n}) = f(\underline{\mathbf{x}}_{k,n}, \underline{r}_{k,n} | \mathbf{z}_{1:n})$  for legacy PMPCs are obtained as

$$\underline{q}(\underline{\mathbf{x}}_{k,n}, 1) = \frac{1}{\underline{C}_{k,n}} \alpha(\underline{\mathbf{x}}_{k,n}, 1) \gamma(\underline{\mathbf{x}}_{k,n}, 1) \quad (37)$$

and  $\underline{q}(\underline{\mathbf{x}}_{k,n}, 0) = \underline{q}_{k,n} f_{\text{D}}(\underline{\mathbf{x}}_{k,n})$  with  $\underline{q}_{k,n} = \frac{1}{\underline{C}_{k,n}} \alpha_{k,n} \gamma_{k,n}$ . The normalization constant is given as  $\underline{C}_{k,n} = \langle \gamma(\underline{\mathbf{x}}_{k,n}, 1) \rangle_{\alpha(\underline{\mathbf{x}}_{k,n}, 1)} + \alpha_{k,n} \gamma_{k,n}$ . The beliefs  $\bar{q}(\bar{\mathbf{y}}_{m,n}) = \bar{q}(\bar{\mathbf{x}}_{m,n}, \bar{r}_{m,n})$  approximating the marginal posterior PDFs  $f(\bar{\mathbf{y}}_{m,n} | \mathbf{z}_{1:n}) = f(\bar{\mathbf{x}}_{m,n}, \bar{r}_{m,n} | \mathbf{z}_{1:n})$  for new PMPCs are obtained as

$$\bar{q}(\bar{\mathbf{x}}_{m,n}, 1) = \frac{1}{\bar{C}_{m,n}} \phi(\bar{\mathbf{x}}_{m,n}, 1) \quad (38)$$

and  $\bar{q}(\bar{\mathbf{x}}_{m,n}, 0) = \bar{q}_{m,n} f_{\text{D}}(\bar{\mathbf{x}}_{m,n})$  with  $\bar{q}_{m,n} = \frac{1}{\bar{C}_{m,n}} \phi_{m,n}$ . The normalization constant is given as  $\bar{C}_{m,n} = \langle \phi(\bar{\mathbf{x}}_{m,n}, 1) \rangle_{1_{\mathbb{R}^{5 \times 1}}(\bar{\mathbf{x}}_{m,n})} + \phi_{m,n}$ . Finally, the belief  $q(\mu_{\text{fa},n})$  approximating the marginal posterior PDF  $f(\mu_{\text{fa},n} | \mathbf{z}_{1:n})$  for the mean FAR is obtained as

$$q(\mu_{\text{fa},n}) = \alpha(\mu_{\text{fa},n}) \prod_{k=1}^{K_{n-1}} \rho_k(\mu_{\text{fa},n}) \prod_{m=1}^{M_n} \kappa_m(\mu_{\text{fa},n}). \quad (39)$$

Since integrations involved in the calculations of the messages and beliefs cannot be obtained analytically, we use a computationally efficient sequential particle-based message passing implementation in line with [30]. Similarly to [8], our sequential particle-based implementation uses a “stacked state” [43] comprising the PMPCs states and the mean FAR state. The resulting complexity scales only linearly in the number of particles.

## VI. EXPERIMENTAL RESULTS

The performance of the BP-MPC-SDE algorithm is validated using both synthetic and real radio measurements. For synthetic measurements, the performance is further compared with the PCRLB [44] and that of the KEST algorithm [25].

### A. Analysis Setup

1) *Common Simulation Setup*: For synthetic and real measurements, the following setup and parameters are commonly used. We assume that MPC dispersion parameters with according velocities and normalized amplitudes evolve independently across time and to each other. More specifically, the state-transition model of  $\underline{\theta}_{k,n}$  (with according velocities  $\underline{v}_{dk,n}$  and  $\underline{v}_{\varphi k,n}$ ) is chosen to be a nearly-constant velocity model. The state-transition model of the normalized amplitude  $\underline{u}_{k,n}$  is chosen to be  $\underline{u}_{k,n} = u_{k,n-1} + \epsilon_{u_{k,n}}$ , where the noise  $\epsilon_{u_{k,n}}$  is iid across  $k$ ,  $n$  and  $h$ , zero-mean, and Gaussian with variance  $\underline{\sigma}_{u_{k,n}}^2$ . Based on the models above, the state-transition model of legacy PMPC state  $\underline{x}_{k,n}$  is collectively defined as  $\underline{x}_{k,n} = \mathbf{F}\underline{x}_{k,n-1} + \Gamma\epsilon_n$ , where the transition matrices  $\mathbf{F} \in \mathbb{R}^{5 \times 5}$  and  $\Gamma \in \mathbb{R}^{5 \times 3}$  are formulated as in [22], [45, Section 6.3.2] with sampling period  $\Delta T = 1$  s. The driving process  $\epsilon_n \in \mathbb{R}^{3 \times 1}$  is iid across  $k$ ,  $n$  and  $h$ , zero-mean and Gaussian with covariance matrix  $\text{diag}\{\underline{\sigma}_d^2, \underline{\sigma}_\varphi^2, \underline{\sigma}_{u_{k,n}}^2\}$ . In addition, the state-transition PDF  $f(\mu_{fa,n} | \mu_{fa,n-1})$  of the mean FAR is given as  $\mu_{fa,n} = \mu_{fa,n-1} + \epsilon_{\mu_{fa,n}}$ , where  $\epsilon_{\mu_{fa,n}}$  is iid across  $n$ , zero-mean, and Gaussian with variance  $\sigma_{fa}^2$ . For computational efficiency of the particle-based implementation, the likelihood function (9) of the normalized amplitude is approximated by

$$f(z_{um,n} | u_{k,n}) = \frac{\frac{1}{\sigma_{u_{k,n}} \sqrt{2\pi}} \exp\left(\frac{-(z_{um,n} - u_{k,n})^2}{2\sigma_{u_{k,n}}^2}\right)}{p_d(u_{k,n})} \quad \text{for } z_{um,n} > u_{de} \quad (40)$$

where  $p_d(u_{k,n}) = Q((u_{th} - u_{k,n})/\sigma_{u_{k,n}})$  is the CDF of a Gaussian distribution. The birth PDF of a new PMPCs  $f_n(\bar{x}_{m,n})$  is assumed to be uniform on the region of interest (RoI), i.e.,  $f_n(\bar{x}_{m,n}) = 1/2\pi d_{\max}$ . The particles for the initial state  $\bar{x}_{m,n}$  of a new PMPC are drawn from a 5-D Gaussian distribution with means  $[z_{dm,n} \ z_{\varphi m,n} \ z_{um,n} \ 0 \ 0]^T$  and variances  $[\bar{\sigma}_{dm,n}^2 \ \bar{\sigma}_{\varphi m,n}^2 \ \bar{\sigma}_{um,n}^2 \ \bar{\sigma}_{v_d}^2 \ \bar{\sigma}_{v_\varphi}^2]^T$ , where  $\bar{\sigma}_{dm,n}^2$ ,  $\bar{\sigma}_{\varphi m,n}^2$  and  $\bar{\sigma}_{um,n}^2$  are state-dependent and computed as shown in Section III-C. The particles for the initial mean FAR  $\mu_{fa,n}$  are drawn from a uniform distribution on  $[0.001, 10]$ .

The simulation parameters are as follows: the survival probability  $p_s = 0.999$ , the existence probability threshold  $p_{de} = 0.5$ , the pruning threshold  $p_{pr} = 10^{-4}$ , the mean number of newly

detected MPCs  $\mu_n = 0.008$  and the maximum number of message passing iterations for DA is  $P = 5000$ .<sup>3</sup>

2) *Metrics*: The performance of different methods is measured using the optimal subpattern assignment (OSPA) metric [46], which can efficiently capture the estimation errors of the model order and MPC states when comparing with the true MPC states at each time. We use cutoff parameters 0.1 m and  $10^\circ$  for distance and AoA respectively and order 2. Note that the association between true MPCs and the estimated MPCs are jointly determined with distances and AoAs. The MPC parameters and cutoff parameters are normalized by the Nyquist bandwidth (0.6 m) and Rayleigh resolution ( $56^\circ$ ) respectively. In addition, we compute the PCRLB [44] as a performance benchmark. The error bounds for distance and AoA at time  $n$  are given as  $\varepsilon_{d,n} = (\frac{\text{tr}[\mathbf{J}_{p_n}^{-1}]_{1:L_n}}{L_n})^{\frac{1}{2}}$  and  $\varepsilon_{\varphi,n} = (\frac{\text{tr}[\mathbf{J}_{p_n}^{-1}]_{L_n+1:2L_n}}{L_n})^{\frac{1}{2}}$  respectively, where  $\mathbf{J}_{p_n}$  denotes the posterior Fisher information matrix (FIM).<sup>4</sup> The mean OSPA (MOSPA) errors, mean distance/AoA error bounds (MEBs) are obtained at each time by averaging over all simulation runs.

### B. Performance for Synthetic Measurements

We assume that a static BS equipped with one antenna transmits  $\tilde{s}(t)$  to a UE equipped with a  $3 \times 3$  uniform rectangular array with an inter-element spacing of 2 cm. Over 364 time instances, 7 MPCs with different lifetimes and time-varying distances and AoAs were synthesized. The amplitude of each MPC is assumed to follow free-space pathloss and is attenuated by 3 dB after each reflection. To validate the resolution and association capabilities of the algorithm, intersecting MPCs are designed at time  $n = 83$ , where distances and amplitudes of two MPCs intersect simultaneously, and AoAs are separated. The noise variance  $\sigma^2$  is specified with a given  $\text{SNR}_{1m} = 10 \log_{10} \left( \frac{|\alpha_{\text{LoS}}|^2 \|\mathbf{s}_{\text{LoS}}\|^2}{\sigma^2} \right)$ , where the amplitude  $\alpha_{\text{LoS}}$  and the signal vector  $\mathbf{s}_{\text{LoS}}$  of the line-of-sight (LoS) path are computed at 1 m distance. Note that the array gain and frequency sample gain are considered in both  $\text{SNR}_{1m}$  and the component SNR  $\text{SNR}_{l,n}$ . For the transmit signal  $\tilde{s}(t)$ , we use a root-raised-cosine pulse with a roll-off factor of 0.6 and duration of  $T_p = 2$  ns (bandwidth of 500 MHz) at a center frequency of  $f_c = 6$  GHz. With sampling period  $T_s = 1.25$  ns, the number of samples per array element is  $N_s = 46$ . In [21], [47], a detection threshold  $u_{\text{de}}$  is determined for SR-SBL channel estimation algorithms for single-snapshot wideband MIMO

<sup>3</sup>The heuristic approach to scale the standard deviation  $\sigma_{u_{k,n}}$  by the MMSE estimates  $u_{n-1}^{\text{MMSE}}$  was chosen since the range of normalized amplitude values tends to be very large.

<sup>4</sup>Note that the OSPA error is normalized by the cardinality of the larger set. Correspondingly, we normalize the error bound with the true number of MPCs  $L_n$ .

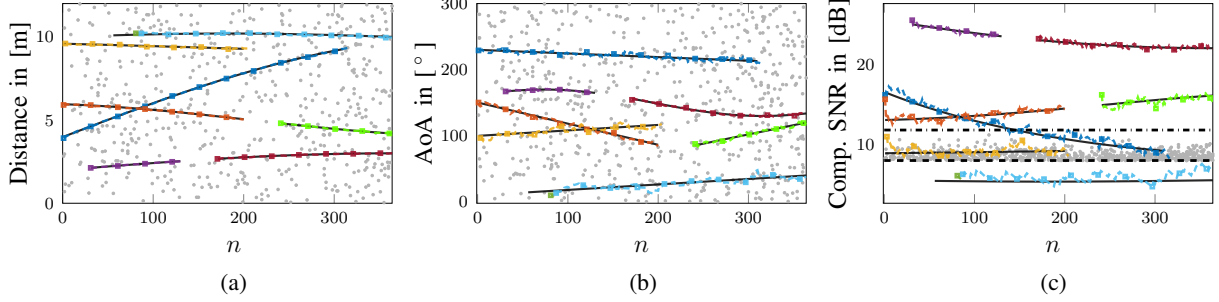


Fig. 3: Results for fully synthetic measurements with the proposed algorithm given  $\text{SNR}_{1m} = 31.5 \text{ dB}$ . Estimates of (a) distance, (b) AoA, (c) component SNR. The black solid lines denote the true MPC parameters. The gray dots denote the false alarm measurements. The estimates of different MPCs are denoted with densely dashed lines with square markers in different colors. The horizontal dashed and dash-dotted lines indicate the thresholds of 8 dB and 11.8 dB respectively.

measurements. Given the signal parameter, number of antennas, and array-layout as defined above, this preprocessing-related detection threshold  $u_{de}$  for a preprocessing-related false alarm probability of  $10^{-2}$  is given as 11.8 dB. MPCs below  $u_{de}$  are mostly miss detected and therefore barely utilized as measurements in the proposed algorithm. To support the sequential detection and estimation of low SNR MPCs, we relax the preprocessing-related detection threshold to  $u_{de} = 8 \text{ dB}$ , which will inevitably bring more false alarm measurements. However, the proposed algorithm can efficiently filter out these false alarms even under low  $\text{SNR}_{1m}$  conditions as shown in the following experimental results. We performed 100 simulation runs for each  $\text{SNR}_{1m} \in \{31.5, 34.5, 39.5, 41.5, 44.5\} \text{ dB}$ . The parameters involved in the BP-MPC-SDE algorithm are:  $d_{\max} = 17 \text{ m}$ ,  $\sigma_d = 0.002 \text{ m/s}^2$ ,  $\sigma_\varphi = 0.17^\circ/\text{s}^2$ ,  $\sigma_{uk,n} = 0.02 u_{k,n-1}^{\text{MMSE}}$ ,  $\sigma_{fa} = 0.74$ ,  $\bar{\sigma}_{v_d} = 0.01 \text{ m/s}$ ,  $\bar{\sigma}_{v_\varphi} = 0.6^\circ/\text{s}$ .

1) *Fully Synthetic Measurements*: We first present the simulation results using fully synthetic measurements without involving the snapshot-based channel estimator. In each simulation run, MPC-oriented measurements were generated by adding Gaussian noises to the true MPC parameters, where the noise variances were state-dependent and computed as in Section III-C. In addition, false alarm measurements were generated with increasing mean FAR  $\mu_{fa,n}$  from 1.5 to 3. More specifically, the distances and AoAs of false alarm measurements were drawn from uniform distributions in the validation region, and the norm amplitudes were generated with Rayleigh distribution with 1/2 spread parameter. Measurements with component SNRs above the threshold of  $u_{de} = 8 \text{ dB}$  were further used in the proposed algorithm.

Fig. 3 shows the results of an exemplary simulation run given the lowest  $\text{SNR}_{1m} = 31.5 \text{ dB}$ . As can be observed, the proposed algorithm exhibits high detection and estimation accuracy for

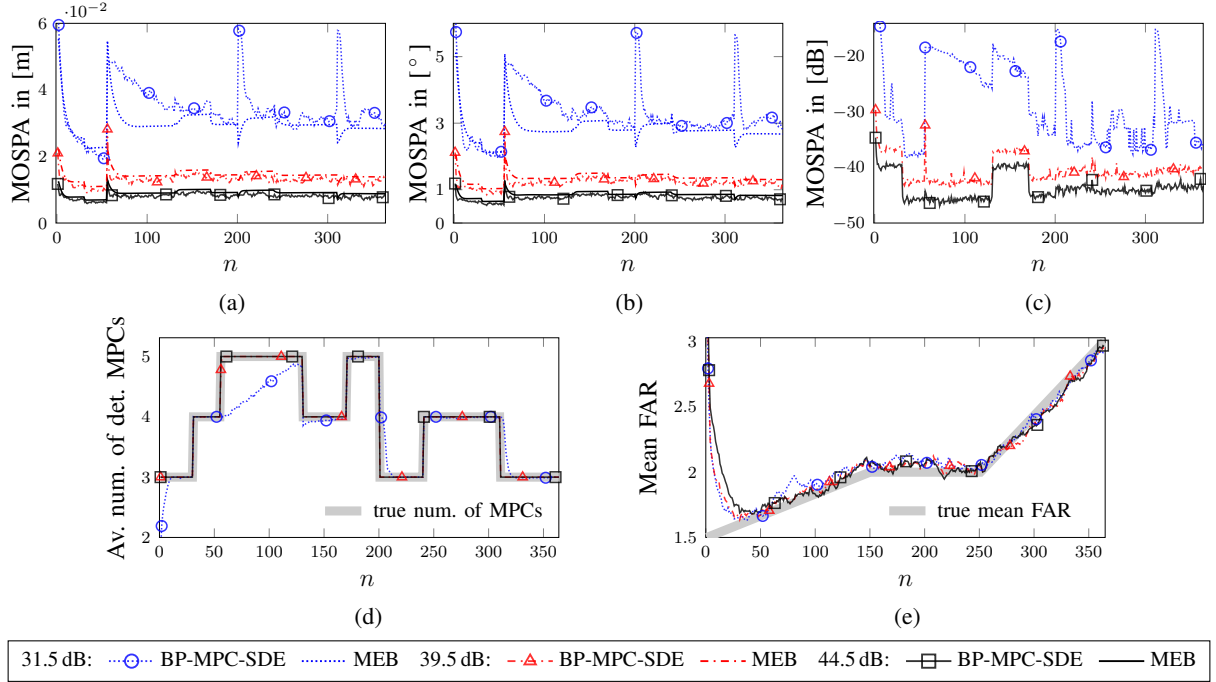


Fig. 4: Results for fully synthetic measurements with the proposed algorithm given  $\text{SNR}_{1m} = \{31.5, 39.5, 44.5\} \text{ dB}$ . MOSPA errors of the estimated (a) distances, (b) AoAs, (c) component SNRs. (d) The average number of detected MPCs. (e) The estimated mean FAR.

the MPCs with medium and high SNRs. Besides, the “weakest” MPC below the threshold of 8 dB is stably detected shortly after the beginning although the related measurements are mostly miss detected in the SR-SBL. The superior detection performance can be explained by the facts that: (i) Using  $u_{de} = 8 \text{ dB}$  enables more often detection of measurements for “weak” MPCs despite bringing dense false alarms; (ii) Exploiting adaptive mean FAR and detection probabilities that are formulated with amplitude information not only results in better differentiation between MPC-oriented measurements and false alarm measurements, but also better maintenance of “weak” MPCs with low SNRs. Additionally, the results show that the proposed algorithm can cope with intersecting MPCs that are close-by in dispersion space by jointly performing probabilistic DA with sequential detection and estimation.

The robustness of the proposed algorithm is further suggested in Fig. 4, where the MOSPA errors, the averaged number of detected MPCs and mean FAR over 100 simulation runs are presented. For medium and high  $\text{SNR}_{1m}$  values, the model order is accurately detected and the MOSPA errors attain the MEBs. For distance, AoA and component SNR, the MOSPA errors are mostly below 2 cm, 2° and  $-35 \text{ dB}$  respectively. Given the lowest  $\text{SNR}_{1m} = 31.5 \text{ dB}$ , the MOSPA errors remain on the MEB-levels mostly, despite the peaks at some time instances due

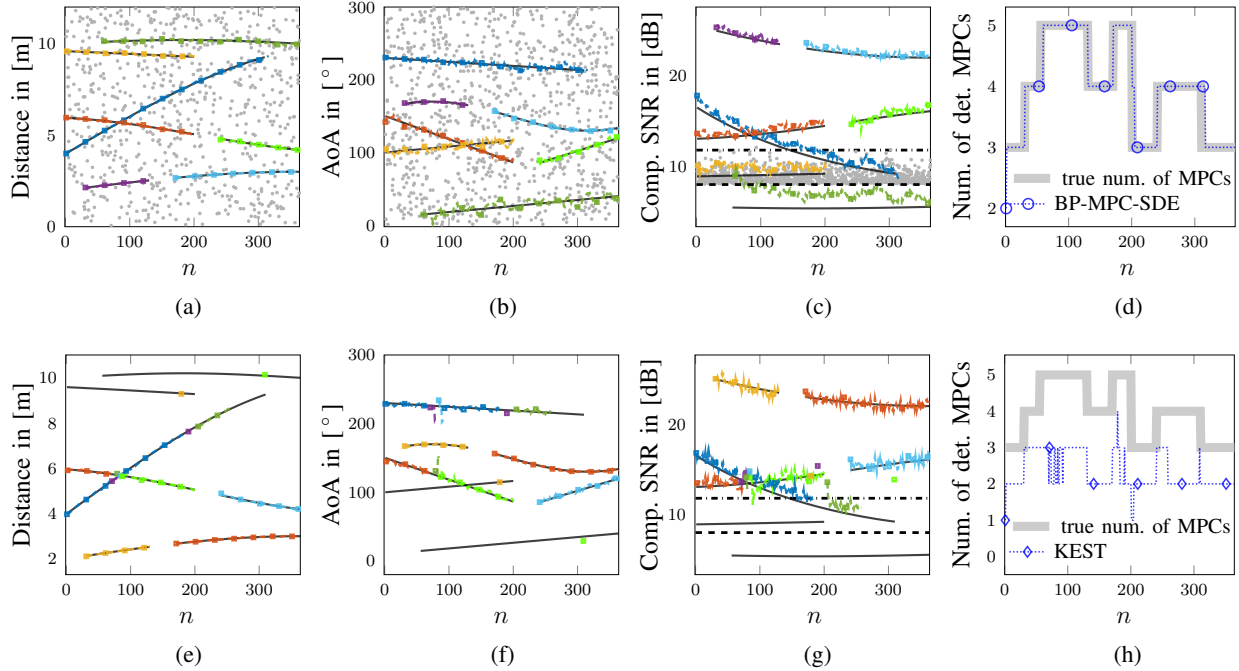


Fig. 5: Results for synthetic radio measurements given  $\text{SNR}_{1m} = 31.5 \text{ dB}$ : (a) to (d) Results of the proposed algorithm, the gray dots denote the false alarm measurements. (e) to (h) Results of the KEST algorithm. The black solid lines denote the true MPC parameters. The gray dots denote the false alarm measurements. The estimates of different MPCs are denoted with densely dashed lines with square markers in different colors. The horizontal dashed and dash-dotted lines indicate the thresholds of 8 dB and 11.8 dB respectively.

to the underestimated model order. Furthermore, the mean FAR is accurately estimated in all conditions.

2) *Synthetic Radio Measurements*: Next, we show the overall performance of the proposed two-stage algorithm by involving the snapshot-based channel estimator. In each simulation run, radio measurements were synthesized by applying the true MPC parameters to the radio signal model (2), where the AWGN was generated with the noise variance  $\sigma^2$  specified by  $\text{SNR}_{1m}$ . The measurements  $z_{m,n}$  at each time  $n$  were provided by a snapshot-based SR-SBL channel estimator in line with the implementation in [35]. For comparison, we implemented the KEST algorithm according to [17], [25] which performs sequential detection and estimation of the distances, AoAs and absolute amplitude of MPCs. Regarding the model order detection in the KEST algorithm, the penalty factors for a higher model order was set to  $p_{\text{ord}} = 0.1$ , and the penalty for a model order change  $p_{\text{chg}}$  was chosen according to the MDL criterion [17], [25].

Fig. 5 presents the results of the proposed algorithm and the KEST algorithm of an exemplary simulation run given  $\text{SNR}_{1m} = 31.5 \text{ dB}$ . When handling well-separated MPCs with high component SNRs, the algorithms perform similarly good. The slightly over estimated component

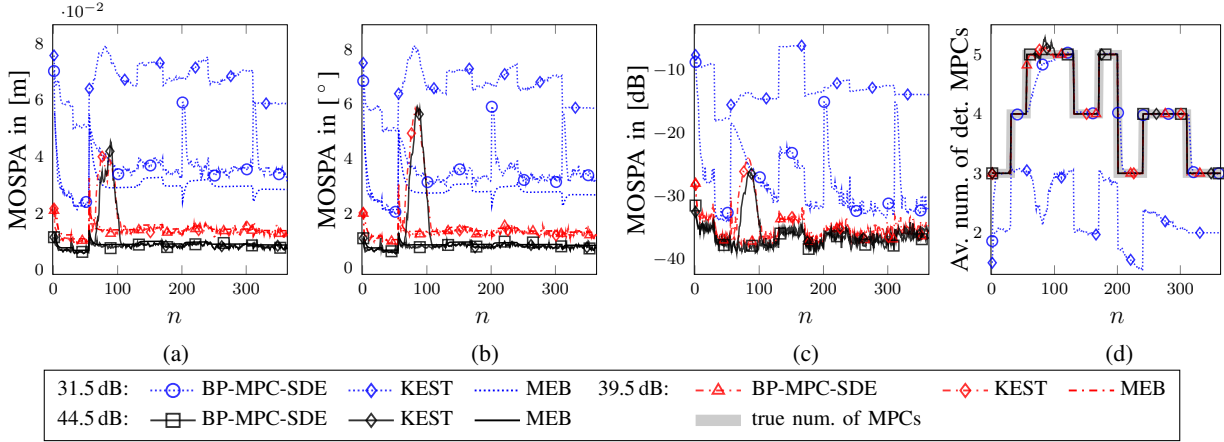


Fig. 6: Results for synthetic radio measurements given  $\text{SNR}_{1m} = \{31.5, 39.5, 44.5\}$  dB. MOSPA errors of the estimated (a) distances, (b) AoAs, (c) component SNRs. (d) The average number of detected MPCs.

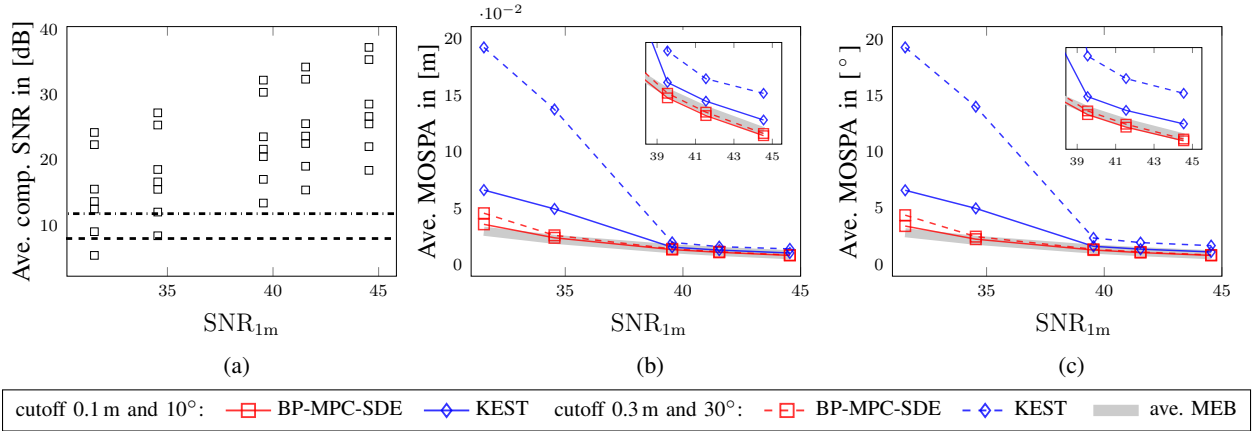


Fig. 7: Results for synthetic radio measurements: (a) The square markers represent the true averaged component SNRs of 7 MPCs. The horizontal dashed and dash-dotted lines indicate the thresholds of 8 dB and 11.8 dB respectively. (b) and (c), the average MOSPA errors and average MEBs for distance and AoA.

SNRs shown in Fig. 5c are due to the Gaussian approximation on the likelihood function (see for Section VI-A1). Regarding the MPC below the threshold of 8 dB, it is immediately detected and accurately estimated in the proposed algorithm but totally missed in the KEST algorithm. Additionally, with probabilistic DA the proposed algorithm properly copes with intersecting MPCs around  $n = 83$ , while the association uncertainty which further leads to discontinuity of sequential estimations is clearly shown with the KEST algorithm.

Fig. 6 shows the MOSPA errors, MEBs and the averaged number of detected MPCs for  $\text{SNR}_{1m} = \{31.5, 39.5, 44.5\}$  dB respectively. The peaks of MOSPA errors indicate the model order estimation error which mostly happen when there are MPC births or deaths. For high  $\text{SNR}_{1m}$  values, it can be observed that the MOSPA errors of the proposed algorithm are mostly

below 2 cm,  $2^\circ$  and  $-35$  dB respectively for distance, AoA and component SNR. The KEST algorithm shows comparable results except for the high error peaks around the intersecting MPCs at time  $n = 83$ . For the lowest  $\text{SNR}_{1m}$ , the MOSPA errors for the proposed algorithm are slightly above the MEBs due to the occasionally missed detection of the “weakest” MPC below the threshold of 8 dB, while the KEST algorithm has much larger MOSPA errors since it does not detect MPCs with low SNR at all (see for Fig. 6d).

Finally, Fig. 7 summarizes the results for all five  $\text{SNR}_{1m} = \{31.5, 34.5, 39.5, 41.5, 44.5\}$  dB values. As expected for the first two values of  $\text{SNR}_{1m}$ , the miss detection of the “weak” MPCs below the threshold of 11.8 dB and even below the threshold of 8 dB as depicted in Fig. 7a with the KEST algorithm results in much higher average MOSPA errors than in the proposed algorithm, as shown in Fig. 7b and Fig. 7c. By setting the cutoff parameters to larger values, i.e., 0.3 m and  $30^\circ$ , the model order estimation error and therefore the average MOSPA errors of the KEST algorithm are better visualized. For high  $\text{SNR}_{1m}$  values where MPCs are mostly detected in both methods, the proposed algorithm still outperforms the KEST algorithm, which can be mainly explained by the much lower MOSPA errors when handling the intersecting MPCs. In summary, the proposed algorithm outperforms the KEST algorithm and attains the average MEBs for almost all  $\text{SNR}_{1m}$  conditions.

### C. Performance for Real Radio Measurements

For further validation of the proposed algorithm, we use real radio measurements collected in a seminar room at TU Graz, Austria. The floor plan is depicted in Fig. 8, including the positions of the static BS and a few mirror images of the BS, i.e., virtual anchors (VAs) which model the MPCs due to specular reflections. More details about the measurement environment and VA computation can be found in [48]. The BS transmitted ultra-wideband signals which were received by the UE at 100 positions along a 2 m trajectory. On the BS side, a dipole-like antenna with an approximately uniform radiation pattern in the azimuth plane and zeros in the floor and ceiling directions was used. At each UE position, a same antenna was mounted on a plotter and moved yielding a virtual uniform rectangular array with an inter-element spacing of 2 cm. The signal was measured using an M-sequence correlative channel sounder with frequency range 3.1–10.6 GHz. We selected a subband signal with bandwidth  $B = 1/T_p$  using filtering with a root-raised-cosine pulse with a roll-off factor of 0.6 and pulse duration  $T_p$  at center frequency of  $f_c = 6$  GHz. Two set of signals were generated with following setups respectively: (i) *setup-*

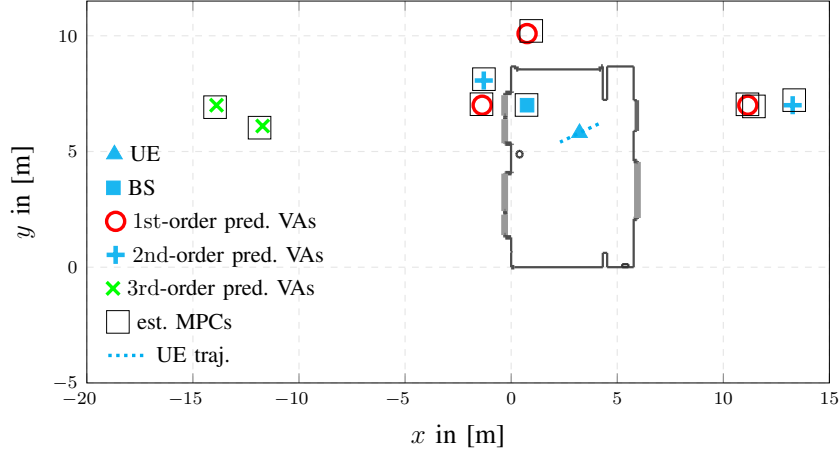


Fig. 8: Floor plan of the measurement environment and the results of the proposed algorithm using real radio measurements of *setup-2* (1 GHz bandwidth and  $5 \times 5$  uniform rectangular array) at time  $n = 50$ . For each of the 12 detected MPC, the estimated distance and AoA are transformed into two dimensional coordinate and associated with a geometrically predicted VAs.

1:  $T_p = 2$  ns,  $B = 0.5$  GHz,  $3 \times 3$  array, (ii) *setup-2*:  $T_p = 1$  ns,  $B = 1$  GHz,  $5 \times 5$  array. Since no significant AWGN was observed from the filtered signal, artificial AWGN generated with  $\text{SNR}_{1m} = 30$  dB was added. The simulation parameters are as follows:  $d_{\max} = 30$  m,  $\sigma_d = 0.03$  m/s $^2$ ,  $\sigma_\varphi = 1^\circ/\text{s}^2$ ,  $\sigma_{u_{k,n}} = 0.1 u_{k,n-1}^{\text{MMSE}}$ ,  $\sigma_{\text{fa}} = 1$ ,  $\bar{\sigma}_{v_d} = 0.1$  m/s,  $\bar{\sigma}_{v_\varphi} = 6^\circ/\text{s}$ , and the preprocessing-related detection threshold  $u_{\text{de}} = 13$  dB for *setup-1* and  $u_{\text{de}} = 17$  dB for *setup-2*.

Fig. 9 shows the estimated delays and AoAs of the detected MPCs for *setup-1* and *setup-2*. The backgrounds of Fig. 9a and Fig. 9b are the delay and angular power spectra versus time respectively for *setup-1*, where the peaks and variations representing individual MPC paths are distinct in delay domain with good resolution capability of ultra-wideband signals, but hardly resolved in angular domain with limited array aperture. As can be observed, some distinct peaks align with the MPC paths predicted with up to 3rd-order geometrically expected VAs, and further associate with the estimated MPC paths highlighted with their respective estimated component SNRs in Fig. 9c and Fig. 9d for *setup-1* and in Fig. 9e and Fig. 9f for *setup-2*. The intersecting 1st-order MPCs and a few short-lived MPCs around 5 m are with parameters nearby in both delay and angular domains. They are better resolved for *setup-2* with larger signal bandwidth and array size, however oscillation on the estimates still exist especially in the angular domain as for *setup-1*. Fig. 8 zooms into the performance of a single snapshot for *setup-2*, where the MMSE estimates of the detected MPC states at time  $n = 50$  after being transformed into two-dimensional coordinates are shown. Within the 12 detected MPCs, the LoS component and MPCs

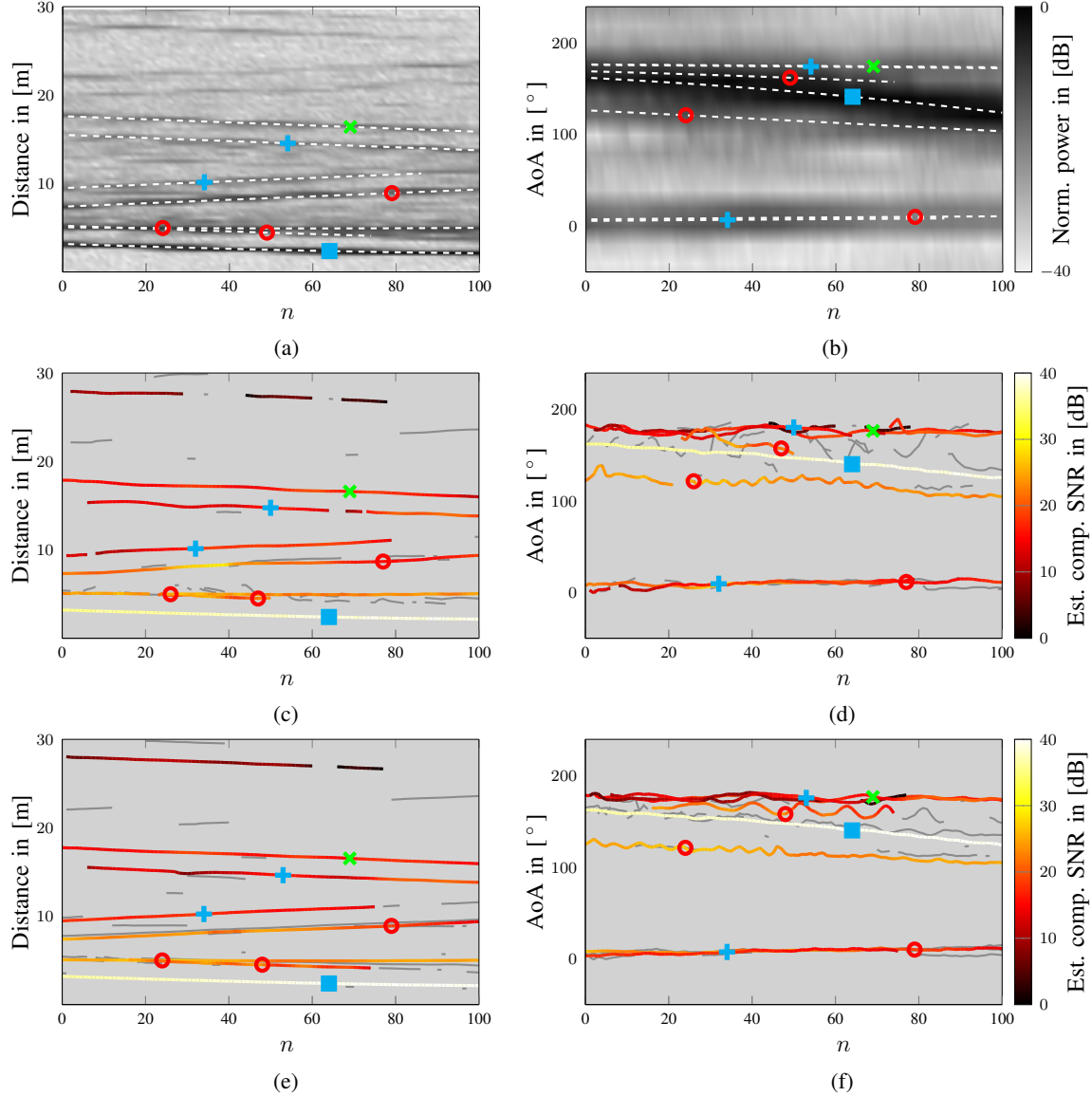


Fig. 9: Results for real radio measurements. (a) and (b) depict the (normalized) delay and angular power spectra of the filtered received signals of *setup-1* versus time, which are basically the same with *setup-2* but with relatively lower delay and angular resolutions. Corresponding to the distinct peaks and their variations in the spectra, a few exemplary distance and AoA paths (white dashed lines) are predicted with geometrically expected VAs, of which the orders are highlighted with markers listed in Fig. 8. The distance and AoA estimates (gray solid lines) of the detected MPCs are shown for *setup-1* in (c) and (d), and for *setup-2* in (e) and (f), among which the estimates associated with the exemplary predicted paths in (a) and (c) are highlighted with their respective estimated component SNRs and markers.

associated with the three 1st-order VAs w.r.t. surrounding walls are accurately estimated. The rest of the detected MPCs are also well explained by some higher order VAs except for the one behind the 1st-order MPC on the right side. Due to imperfect hardware calibration leading to dispersive system response, shadow components are sometimes detected alongside significant

MPCs. In addition, the estimated MPC associated with the 2nd-order VA on the upper left side represents the reflections between complex room structure on the corner. Note that the wall on the lower side has high attenuation factor, thus the associated MPCs are very weak in amplitude and hardly detected. In summary, the proposed algorithm detects specular MPC and estimates their parameters that well represent the geometrical truth and dynamic behaviors of the radio channel.

## VII. CONCLUSIONS

We proposed a BP-based message passing algorithm for sequential detection and estimation of MPC parameters based on radio signals. Our algorithm adopts a two-stage structure combining a snapshot-based SR-SBL channel estimator with a BP-based sequential detection and estimation algorithm. The proposed algorithm exploits the normalized amplitude measurements to determine the detection probabilities related to the PMPCs states. It is therefore also suitable for unknown and time-varying detection probabilities. It also estimates the possibly time-varying mean number of false alarms. The utilization of normalized amplitudes and the augmentation of PMPCs state with binary existence variable enables the reliable detection of “weak” MPCs with very low component SNR and the accurate estimation of their parameters. Furthermore, the algorithm excellently copes with intersecting MPCs, i.e., MPCs with parameters nearby in the dispersion space by performing joint DA and sequential detection/estimation. Simulation results using synthetic measurements show that the proposed algorithm estimates the parameters of MPC on PCRLB-level even for MPC with very low SNR and outperforms state-of-the-art algorithms in that sense. The results using real radio measurements are with high accuracy which further demonstrates the excellent performance of the algorithm even in real challenging environments.

## APPENDIX

### A. The Joint Prior PDF

At first, a few sets are defined as follows:  $\mathcal{N}_{\bar{r}_n} \triangleq \{m \in \{1, \dots, M_n\} : \bar{r}_{m,n} = 1, b_{m,n} = 0\}$  denotes the existing new PMPCs set, and  $\mathcal{D}_{a_n, \underline{r}_n} \triangleq \{k \in \{1, \dots, K_{n-1}\} : \underline{r}_{k,n} = 1, a_{k,n} \neq 0\}$  denotes the existing legacy PMPCs set. Correspondingly, the sets of non-existing new PMPCs are given as  $\overline{\mathcal{N}}_{\bar{r}_n} \triangleq \{1, \dots, M_n\} \setminus \mathcal{N}_{\bar{r}_n}$ , and the sets of non-existing legacy PMPCs are given as  $\overline{\mathcal{D}}_{a_n, \underline{r}_n} \triangleq \{1, \dots, K_{n-1}\} \setminus \mathcal{D}_{a_n, \underline{r}_n}$ . Hence, the number of false alarm measurements can be

represented with the sets as  $k_{\text{fa},n} = M_n - |\mathcal{D}_{\mathbf{a}_n, \underline{\mathbf{r}}_n}| - |\mathcal{N}_{\bar{\mathbf{r}}_n}|$ , and the number of PMPCs states is given as  $K_{n-1} + M_n = |\mathcal{D}_{\mathbf{a}_n, \underline{\mathbf{r}}_n}| + |\bar{\mathcal{D}}_{\mathbf{a}_n, \underline{\mathbf{r}}_n}| + |\mathcal{N}_{\bar{\mathbf{r}}_n}| + |\bar{\mathcal{N}}_{\bar{\mathbf{r}}_n}|$ .

Before the current measurements are observed, the number of measurements  $M_n$  is random. The Poisson PMF of the number of existing new PMPCs evaluated at  $|\mathcal{N}_{\bar{\mathbf{r}}_n}|$  is given by  $p(|\mathcal{N}_{\bar{\mathbf{r}}_n}|) = \mu_n^{|\mathcal{N}_{\bar{\mathbf{r}}_n}|}/|\mathcal{N}_{\bar{\mathbf{r}}_n}|!e^{\mu_n}$ . The prior PDF of the new PMPC state  $\bar{\mathbf{x}}_n$  conditioned on  $\bar{\mathbf{r}}_n$  and  $M_n$  (where the number of measurements is random) is expressed as

$$f(\bar{\mathbf{x}}_n | \bar{\mathbf{r}}_n, M_n) = \prod_{m \in \mathcal{N}_{\bar{\mathbf{r}}_n}} f_n(\bar{\mathbf{x}}_{m,n}) \prod_{m' \in \bar{\mathcal{N}}_{\bar{\mathbf{r}}_n}} f_D(\bar{\mathbf{x}}_{m',n}). \quad (41)$$

After observing the measurements  $\mathbf{z}_n$  at time  $n$ , the number of new PMPCs is  $M_n$ .

The PMF for the number of false alarm measurements is given by  $p(k_{\text{fa},n}) = \mu_{\text{fa},n}^{k_{\text{fa},n}}/k_{\text{fa},n}!e^{\mu_{\text{fa},n}}$ . The joint conditional prior PMF of the binary existence variables of new PMPCs  $\bar{\mathbf{r}}_n \triangleq [\bar{r}_{1,n} \cdots \bar{r}_{M_n,n}]$ , the DA vectors  $\mathbf{a}_n$  and  $\mathbf{b}_n$  and the number of the measurements  $M_n$  conditioned on  $\mu_{\text{fa},n}$  and  $\underline{\mathbf{y}}_n$  is obtained as [8], [26], [27]

$$\begin{aligned} p(\bar{\mathbf{r}}_n, \mathbf{a}_n, \mathbf{b}_n, M_n | \mu_{\text{fa},n}, \underline{\mathbf{y}}_n) &= \chi_{\bar{\mathbf{r}}_n, \mathbf{a}_n, M_n} \left( \prod_{m \in \mathcal{N}_{\bar{\mathbf{r}}_n}} \Gamma_{\mathbf{a}_n}(\bar{r}_{m,n}) \right) \left( \prod_{k \in \mathcal{D}_{\mathbf{a}_n, \underline{\mathbf{r}}_n}} p_d(\underline{u}_{k,n}) \right) \Psi(\mathbf{a}_n, \mathbf{b}_n) \\ &\times \left( \prod_{k' \in \bar{\mathcal{D}}_{\mathbf{a}_n, \underline{\mathbf{r}}_n}} (1(a_{k',n}) - \underline{r}_{k',n} p_d(\underline{u}_{k',n})) \right) \end{aligned} \quad (42)$$

where the normalization constant  $\chi_{\bar{\mathbf{r}}_n, \mathbf{a}_n, M_n} = e^{-(\mu_{\text{fa},n} + \mu_n)} \mu_n^{|\mathcal{N}_{\bar{\mathbf{r}}_n}|} \mu_{\text{fa},n}^{k_{\text{fa},n}} / M_n!$  depends on both  $\mu_{\text{fa},n}$  and  $\mu_n$ . Since the mean number of newly detected MPCs  $\mu_n$  is assumed to be a known constant, we introduce another normalization constant  $n(\mu_{\text{fa},n}) \triangleq (\mu_{\text{fa},n}^{M_n} e^{-\mu_{\text{fa},n}} / M_n!)^{1/(K_{n-1} + M_n)}$  which is related to  $\mu_{\text{fa},n}$  only. The two exclusion functions  $\Psi(\mathbf{a}_n, \mathbf{b}_n)$  and  $\Gamma_{\mathbf{a}_n}(\bar{r}_{m,n}) = 0$  ensures that  $p(\bar{\mathbf{r}}_n, \mathbf{a}_n, \mathbf{b}_n, M_n | \mu_{\text{fa},n}, \underline{\mathbf{y}}_n) \neq 0$  if and only if a measurement is generated from no more than one PMPC (either a legacy or a new one), and a PMPC generates no more than one measurement.

Assuming that the new PMPCs states  $\bar{\mathbf{y}}_n$  and the PMPC-oriented association variables  $\mathbf{a}_n$  are conditionally independent given the legacy PMPCs state  $\underline{\mathbf{y}}_n$ . The joint prior PDF of  $\underline{\mathbf{y}}_{1:n}$ ,  $\bar{\mathbf{y}}_{1:n}$ ,  $\mathbf{a}_{1:n}$ ,  $\mathbf{b}_{1:n}$ ,  $\mu_{\text{fa},1:n}$ , and the number of the measurements  $\mathbf{m}_{1:n}$  is then given as

$$\begin{aligned} f(\mathbf{y}_{1:n}, \mathbf{a}_{1:n}, \mathbf{b}_{1:n}, \mu_{\text{fa},1:n}, \mathbf{m}_{1:n}) &= f(\underline{\mathbf{y}}_{1:n}, \bar{\mathbf{y}}_{1:n}, \mathbf{a}_{1:n}, \mathbf{b}_{1:n}, \mu_{\text{fa},1:n}, \mathbf{m}_{1:n}) \\ &= f(\mu_{\text{fa},1}) f(\bar{\mathbf{x}}_1 | \bar{\mathbf{r}}_1, M_1) p(\bar{\mathbf{r}}_1, \mathbf{a}_1, \mathbf{b}_1, M_1 | \mu_{\text{fa},1}) \prod_{n'=2}^n f(\mu_{\text{fa},n'} | \mu_{\text{fa},n'-1}) \end{aligned}$$

$$\times \left( \prod_{k=1}^{K_{n'-1}} f(\underline{\mathbf{y}}_{k,n'} | \mathbf{y}_{k,n'-1}) \right) f(\bar{\mathbf{x}}_{n'} | \bar{\mathbf{r}}_{n'}, M_{n'}) p(\bar{\mathbf{r}}_{n'}, \mathbf{a}_{n'}, \mathbf{b}_{n'}, M_{n'} | \mu_{\text{fa},n'}, \underline{\mathbf{y}}_{n'}) \quad (43)$$

where  $p(\bar{\mathbf{r}}_1, \mathbf{a}_1, \mathbf{b}_1, M_1 | \mu_{\text{fa},1}, \underline{\mathbf{y}}_1) = p(\bar{\mathbf{r}}_1, \mathbf{a}_1, \mathbf{b}_1, M_1 | \mu_{\text{fa},1})$  since no legacy PMPC exist at time  $n = 1$ .

In (43) the product of the joint conditional prior PMF (42) and the prior PDF of new PMPCs (41) is given by

$$\begin{aligned} p(\bar{\mathbf{r}}_n, \mathbf{a}_n, \mathbf{b}_n, M_n | \mu_{\text{fa},n}, \underline{\mathbf{y}}_n) f(\bar{\mathbf{x}}_n | \bar{\mathbf{r}}_n, M_n) &\propto \left( \prod_{k=1}^{K_{n-1}} g_1(\underline{\mathbf{y}}_{k,n}, a_{k,n}, \mu_{\text{fa},n}; M_n) \prod_{m=1}^{M_n} \psi(a_{k,n}, b_{m,n}) \right) \\ &\times \left( \prod_{m=1}^{M_n} h_1(\bar{\mathbf{y}}_{m,n}, b_{m,n}, \mu_{\text{fa},n}; M_n) \right) \end{aligned} \quad (44)$$

with  $g_1(\underline{\mathbf{y}}_{k,n}, a_{k,n}, \mu_{\text{fa},n}; M_n) = g_1(\underline{\mathbf{x}}_{k,n}, r_{k,n}, a_{k,n}, \mu_{\text{fa},n}; M_n)$  is given by

$$g_1(\underline{\mathbf{x}}_{k,n}, r_{n,k} = 1, a_{k,n}, \mu_{\text{fa},n}; M_n) \triangleq \begin{cases} \frac{n(\mu_{\text{fa},n}) p_{\text{d}}(\underline{u}_{k,n})}{\mu_{\text{fa},n}}, & a_{k,n} = m \\ 1 - p_{\text{d}}(\underline{u}_{k,n}), & a_{k,n} = 0 \end{cases} \quad (45)$$

and  $g_1(\underline{\mathbf{x}}_{k,n}, r_{k,n} = 0, a_{k,n}, \mu_{\text{fa},n}; M_n) \triangleq \bar{1}(a_{k,n}) n(\mu_{\text{fa},n})$  and  $h_1(\bar{\mathbf{y}}_{m,n}, b_{m,n}, \mu_{\text{fa},n}; M_n) = h_1(\bar{\mathbf{x}}_{m,n}, \bar{r}_{m,n}, b_{m,n}, \mu_{\text{fa},n}; M_n)$  is given by

$$h_1(\bar{\mathbf{x}}_{m,n}, \bar{r}_{m,n} = 1, b_{m,n}, \mu_{\text{fa},n}; M_n) \triangleq \begin{cases} 0, & b_{m,n} = k \\ \frac{n(\mu_{\text{fa},n}) \mu_{\text{n}} f_{\text{n}}(\bar{\mathbf{x}}_{m,n})}{\mu_{\text{fa},n}}, & b_{m,n} = 0 \end{cases} \quad (46)$$

and  $h_1(\bar{\mathbf{x}}_{m,n}, \bar{r}_{m,n} = 0, b_{m,n}, \mu_{\text{fa},n}; M_n) \triangleq n(\mu_{\text{fa},n})$ . By inserting (44) into (43), the *joint prior PDF* can be rewritten as

$$\begin{aligned} &f(\underline{\mathbf{y}}_{1:n}, \bar{\mathbf{y}}_{1:n}, \mathbf{a}_{1:n}, \mathbf{b}_{1:n}, \mu_{\text{fa},1:n}, \mathbf{m}_{1:n}) \\ &\propto f(\mu_{\text{fa},1}) \prod_{l=1}^{M_1} h_1(\bar{\mathbf{y}}_{l,1}, \mu_{\text{fa},1}; M_1) \prod_{n'=2}^n f(\mu_{\text{fa},n'} | \mu_{\text{fa},n'-1}) \left( \prod_{k'=1}^{K_{n'-1}} f(\underline{\mathbf{y}}_{k',n'} | \mathbf{y}_{k',n'-1}) \right) \\ &\times \left( \prod_{k=1}^{K_{n'-1}} g_1(\underline{\mathbf{y}}_{k,n'}, a_{k,n'}, \mu_{\text{fa},n'}; M_{n'}) \prod_{m=1}^{M_{n'}} \psi(a_{k,n'}, b_{m,n'}) \right) \left( \prod_{m'=1}^{M_{n'}} h_1(\bar{\mathbf{y}}_{m',n'}, b_{m',n'}, \mu_{\text{fa},n'}; M_{n'}) \right). \end{aligned} \quad (47)$$

### B. The Joint Likelihood Function

Assume that the measurements  $\mathbf{z}_n$  are independent across  $n$ , the conditional PDF of  $\mathbf{z}_{1:n}$  given  $\underline{\mathbf{y}}_{1:n}$ ,  $\bar{\mathbf{y}}_{1:n}$ ,  $\mathbf{a}_{1:n}$ ,  $\mathbf{b}_{1:n}$ , and the number of the measurements  $\mathbf{m}_{1:n}$  is given by

$$f(\mathbf{z}_{1:n} | \underline{\mathbf{y}}_{1:n}, \bar{\mathbf{y}}_{1:n}, \mathbf{a}_{1:n}, \mathbf{b}_{1:n}, \mathbf{m}_{1:n}) = \prod_{n'=1}^n f(\mathbf{z}_{n'} | \underline{\mathbf{y}}_{n'}, \bar{\mathbf{y}}_{n'}, \mathbf{a}_{n'}, \mathbf{b}_{n'}, M_{n'}). \quad (48)$$

Note that  $f(\mathbf{z}_1 | \underline{\mathbf{y}}_1, \bar{\mathbf{y}}_1, \mathbf{a}_1, \mathbf{b}_1, M_1) = f(\mathbf{z}_1 | \bar{\mathbf{y}}_1, \mathbf{a}_1, \mathbf{b}_1, M_1)$  since there is no legacy PMPC at time  $n = 1$ . The conditional PDF  $f(\mathbf{z}_{m,n} | \mathbf{x}_{k,n})$  characterizing the statistical relation between the measurements  $\mathbf{z}_{m,n}$  and the PMPC states  $\mathbf{x}_{k,n}$ . This PDF is a central element in the conditional PDF of the measurement vector  $\mathbf{z}_n$  given  $\underline{\mathbf{y}}_n$ ,  $\bar{\mathbf{y}}_n$ ,  $\mathbf{a}_n$ ,  $\mathbf{b}_n$ , and the number of the measurements  $M_n$ . Assuming that the  $\mathbf{z}_{m,n}$  are conditionally independent across  $m$  given  $\underline{\mathbf{y}}_{k,n}$ ,  $\bar{\mathbf{y}}_{m,n}$ ,  $\mathbf{a}_{k,n}$ ,  $\mathbf{b}_{m,n}$ , and  $M_n$  [26], we obtain

$$\begin{aligned} f(\mathbf{z}_{1:n} | \underline{\mathbf{y}}_{1:n}, \bar{\mathbf{y}}_{1:n}, \mathbf{a}_{1:n}, \mathbf{b}_{1:n}, \mathbf{m}_{1:n}) &= C(\mathbf{z}_1) \left( \prod_{m \in \mathcal{N}_{\bar{\mathbf{r}}_1}} \frac{f(\mathbf{z}_{m,1} | \bar{\mathbf{x}}_{m,1})}{f_{\text{fa}}(\mathbf{z}_{m,1})} \right) \prod_{n'=2}^n C(\mathbf{z}_{n'}) \\ &\quad \times \left( \prod_{k \in \mathcal{D}_{\mathbf{a}_{n'}, \mathbf{r}_{n'}}} \frac{f(\mathbf{z}_{a_{k,n'}, n'} | \underline{\mathbf{x}}_{k,n'})}{f_{\text{fa}}(\mathbf{z}_{a_{k,n'}, n'})} \right) \left( \prod_{m \in \mathcal{N}_{\bar{\mathbf{r}}_{n'}}} \frac{f(\mathbf{z}_{m,n'} | \bar{\mathbf{x}}_{m,n'})}{f_{\text{fa}}(\mathbf{z}_{m,n'})} \right) \end{aligned} \quad (49)$$

where the normalization factor  $C(\mathbf{z}_n) = \prod_{m=1}^{M_n} f_{\text{fa}}(\mathbf{z}_{m,n})$  depends on  $\mathbf{z}_n$  and  $M_n$ , which are both fixed after the current measurement  $\mathbf{z}_n$  is observed. The likelihood function at time  $n$  is further factorized as [26]

$$f(\mathbf{z}_n | \underline{\mathbf{y}}_n, \bar{\mathbf{y}}_n, \mathbf{a}_n, \mathbf{b}_n, M_n) = C(\mathbf{z}_n) \left( \prod_{k \in \mathcal{D}_{\mathbf{a}_n, \mathbf{r}_n}} \frac{f(\mathbf{z}_{a_{k,n}, n} | \underline{\mathbf{x}}_{k,n})}{f_{\text{fa}}(\mathbf{z}_{a_{k,n}, n})} \right) \left( \prod_{m \in \mathcal{N}_{\bar{\mathbf{r}}_n}} \frac{f(\mathbf{z}_{m,n} | \bar{\mathbf{x}}_{m,n})}{f_{\text{fa}}(\mathbf{z}_{m,n})} \right). \quad (50)$$

Since the normalization factor  $C(\mathbf{z}_n)$  is fixed after the current measurement  $\mathbf{z}_n$  is observed, the likelihood function in (50) can be rewritten up to the normalization constant

$$f(\mathbf{z}_n | \underline{\mathbf{y}}_n, \bar{\mathbf{y}}_n, \mathbf{a}_n, \mathbf{b}_n, M_n) \propto \left( \prod_{k=1}^{K_{n-1}} g_2(\underline{\mathbf{y}}_{k,n}, a_{k,n}; \mathbf{z}_n) \right) \left( \prod_{m=1}^{M_n} h_2(\bar{\mathbf{y}}_{m,n}, b_{m,n}; \mathbf{z}_n) \right) \quad (51)$$

where the factor related to legacy PMPC states  $g_2(\underline{\mathbf{y}}_{k,n}, a_{k,n}; \mathbf{z}_n) = g_2(\underline{\mathbf{x}}_{k,n}, \underline{r}_{k,n}, a_{k,n}; \mathbf{z}_n)$  is given by

$$g_2(\underline{\mathbf{x}}_{k,n}, \underline{r}_{k,n} = 1, a_{k,n}; \mathbf{z}_n) \triangleq \begin{cases} \frac{f(\mathbf{z}_{m,n} | \underline{\mathbf{x}}_{k,n})}{f_{\text{fa}}(\mathbf{z}_{m,n})}, & a_{k,n} = m \\ 1, & a_{k,n} = 0 \end{cases} \quad (52)$$

and  $g_2(\underline{\mathbf{x}}_{k,n}, \underline{r}_{k,n} = 0, a_{k,n}; \mathbf{z}_n) \triangleq 1$  and the factor related to new PMPC states  $h_2(\bar{\mathbf{y}}_{m,n}, b_{m,n}; \mathbf{z}_n) = h_2(\bar{\mathbf{x}}_{m,n}, \bar{r}_{m,n}, b_{m,n}; \mathbf{z}_n)$  is given by

$$h_2(\bar{\mathbf{x}}_{m,n}, \bar{r}_{m,n} = 1, b_{m,n}; \mathbf{z}_n) \triangleq \begin{cases} 1, & b_{m,n} = k \\ \frac{f(\mathbf{z}_{m,n} | \bar{\mathbf{x}}_{m,n})}{f_{\text{fa}}(\mathbf{z}_{m,n})}, & b_{m,n} = 0 \end{cases} \quad (53)$$

and  $h_2(\bar{\mathbf{x}}_{m,n}, \bar{r}_{m,n} = 0, b_{m,n}; \mathbf{z}_n) \triangleq 1$ . Inserting (45), (46) and (51) into (48), the conditional PDF (49) can be rewritten as the *joint likelihood function*

$$\begin{aligned} & f(\mathbf{z}_{1:n} | \underline{\mathbf{y}}_{1:n}, \bar{\mathbf{y}}_{1:n}, \mathbf{a}_{1:n}, \mathbf{b}_{1:n}, \mathbf{m}_{1:n}) \\ & \propto \left( \prod_{m'=1}^{M_1} h_2(\bar{\mathbf{x}}_{m',1}, \bar{r}_{m',1}, b_{m',1}; \mathbf{z}_1) \right) \prod_{n'=2}^n \left( \prod_{k=1}^{K_{n'-1}} g_1(\underline{\mathbf{x}}_{k,n'}, \underline{r}_{k,n'}, a_{k,n'}; \mathbf{z}_{n'}) \right) \\ & \quad \times \left( \prod_{m=1}^{M_{n'}} h_1(\bar{\mathbf{x}}_{m,n'}, \bar{r}_{m,n'}, b_{m,n'}; \mathbf{z}_{n'}) \right). \end{aligned} \quad (54)$$

### C. The Joint Posterior PDF

Finally, by substituting the *joint prior PDF* with (47) and the *joint likelihood function* with (54), the *joint posterior PDF* can be rewritten as

$$\begin{aligned} & f(\mathbf{y}_{1:n}, \mathbf{a}_{1:n}, \mathbf{b}_{1:n}, \boldsymbol{\mu}_{\text{fa},1:n}, \mathbf{m}_{1:n} | \mathbf{z}_{1:n}) \\ & = f(\underline{\mathbf{y}}_{1:n}, \bar{\mathbf{y}}_{1:n}, \mathbf{a}_{1:n}, \mathbf{b}_{1:n}, \boldsymbol{\mu}_{\text{fa},1:n}, \mathbf{m}_{1:n} | \mathbf{z}_{1:n}) \\ & \propto f(\boldsymbol{\mu}_{\text{fa},1}) \left( \prod_{l=1}^{M_1} h_1(\bar{\mathbf{y}}_{l,1}, b_{l,1}; \mathbf{z}_1) h_2(\bar{\mathbf{y}}_{l,1}, b_{l,1}, \boldsymbol{\mu}_{\text{fa},1}; M_1) \right) \prod_{n'=2}^n f(\boldsymbol{\mu}_{\text{fa},n'} | \boldsymbol{\mu}_{\text{fa},n'-1}) \\ & \quad \times \left( \prod_{k'=1}^{K_{n'-1}} f(\underline{\mathbf{y}}_{k',n'} | \mathbf{y}_{k',n'-1}) \right) \left( \prod_{k=1}^{K_{n'-1}} g_1(\underline{\mathbf{y}}_{k,n'}, a_{k,n'}, \boldsymbol{\mu}_{\text{fa},n'}; M_{n'}) g_2(\underline{\mathbf{y}}_{k,n'}, a_{k,n'}; \mathbf{z}_{n'}) \psi(a_{k,n'}, b_{m,n'}) \right) \\ & \quad \times \left( \prod_{m'=1}^{M_{n'}} h_1(\bar{\mathbf{y}}_{m',n'}, b_{m',n'}, \boldsymbol{\mu}_{\text{fa},n'}; M_{n'}) h_2(\bar{\mathbf{y}}_{m',n'}, b_{m',n'}; \mathbf{z}_{n'}) \right). \end{aligned} \quad (55)$$

The function related to the legacy PMPCs can be simplified as  $g(\underline{\mathbf{y}}_{k,n}, a_{k,n}, \mu_{\text{fa},n}; \mathbf{z}_n) \triangleq g_1(\underline{\mathbf{y}}_{k,n}, a_{k,n}, \mu_{\text{fa},n}; M_n)g_2(\underline{\mathbf{y}}_{k,n}, a_{k,n}; \mathbf{z}_n)$ , and the function related to the new PMPCs as  $h(\bar{\mathbf{y}}_{m,n}, b_{m,n}, \mu_{\text{fa},n}; \mathbf{z}_n) \triangleq h_1(\bar{\mathbf{y}}_{m,n}, b_{m,n}, \mu_{\text{fa},n}; M_n)h_2(\bar{\mathbf{y}}_{m,n}, b_{m,n}; \mathbf{z}_n)$ .

#### D. The Normalized Amplitude Variance

In this section, we derive the normalized amplitude variance for the likelihood functions introduced in the Section III-C. If the noise variance  $\sigma^2$  is assumed to be known, the statistic of the *PMPC-oriented* normalized amplitude measurement  $z_{\text{u}m,n}$  is described by a Rician distribution with a spread parameter of 1/2. However, since the noise variance is not known a priori it needs to be estimated by the snapshot-based estimator leading to a significant increase of the normalized amplitude spread compared to the spread of 1/2. For large amplitudes and for large  $N_s H$ , the normalized amplitude statistic is well approximated by a Gaussian distribution and the according variance can be determined by the Fisher information [42], [49].<sup>5</sup> For simplification, we assume that the MPCs are well separated in dispersion space, so that their mutual correlation is negligible. We first show the FIM for parameter vector  $\boldsymbol{\xi}_{l,n} = [\Re\{\tilde{\alpha}_{l,n}\} \ \Im\{\tilde{\alpha}_{l,n}\} \ \sigma^2]^T$ , where  $\Re\{\tilde{\alpha}_{l,n}\}$  and  $\Im\{\tilde{\alpha}_{l,n}\}$  denote the real and imaginary parts of the complex amplitudes  $\tilde{\alpha}_{l,n}$ , respectively and then apply the chain rule [42] to find the FIM for  $\tilde{u}_{l,n}$ . According to [42], the elements of the FIM for  $\tilde{\boldsymbol{\xi}}_{l,n}$  are given as

$$[\mathbf{J}_{l,n}(\boldsymbol{\xi}_{l,n})]_{i,j} = 2\Re \left\{ \frac{\partial \tilde{\alpha}_{l,n} \mathbf{s}^H(\tilde{\boldsymbol{\theta}}_{l,n})}{\partial [\xi_{l,n}]_i} \mathbf{C}^{-1} \frac{\partial \mathbf{s}(\tilde{\boldsymbol{\theta}}_{l,n}) \tilde{\alpha}_{l,n}}{\partial [\xi_{l,n}]_j} \right\} + \text{tr} \left\{ \mathbf{C}^{-1} \frac{\partial \mathbf{C}^{-1}}{\partial [\xi_{l,n}]_i} \mathbf{C}^{-1} \frac{\partial \mathbf{C}^{-1}}{\partial [\xi_{l,n}]_j} \right\} \quad (56)$$

where  $i, j \in \{1, 2, 3\}$ . After some straightforward calculations (56) can be rewritten as

$$\mathbf{J}_{l,n}(\boldsymbol{\xi}_{l,n}) = \text{diag} \left\{ \frac{2\|\mathbf{s}(\tilde{\boldsymbol{\theta}}_{l,n})\|^2}{\sigma^2}, \frac{2\|\mathbf{s}(\tilde{\boldsymbol{\theta}}_{l,n})\|^2}{\sigma^2}, \frac{N_s H}{\sigma^4} \right\}. \quad (57)$$

The CRLB for  $\tilde{u}_{l,n}$  is obtained by applying the chain rule, i.e.,

$$\sigma_{\text{u}l,n}^2 \triangleq J_{\tilde{u}l,n}^{-1}(\tilde{u}_{l,n}) = \mathbf{t}_{l,n}^H \mathbf{J}_{l,n}^{-1}(\boldsymbol{\xi}_{l,n}) \mathbf{t}_{l,n} = \frac{1}{2} + \frac{\tilde{u}_{l,n}^2}{4N_s H} \quad (58)$$

where the Jacobian  $\mathbf{t}_{l,n}$  containing the partial derivatives is

$$\mathbf{t}_{l,n} \triangleq \left[ \frac{\partial \tilde{u}_{l,n}}{\partial \Re\{\tilde{\alpha}_{l,n}\}} \quad \frac{\partial \tilde{u}_{l,n}}{\partial \Im\{\tilde{\alpha}_{l,n}\}} \quad \frac{\partial \tilde{u}_{l,n}}{\partial \sigma^2} \right]^T$$

<sup>5</sup>Note that for unknown noise variance the distribution of the normalized amplitude measurement  $z_{\text{u}m,n}$  is not described by a well-known standard distribution anymore. More specifically, the statistic of the squared PMPC-oriented normalized amplitude measurements  $2z_{\text{u}m,n}^2$  is described by a non-central Fisher distribution [50]–[52]. For large  $N_s H$ , the statistic of  $2z_{\text{u}m,n}^2$  can be well approximated by a non-central  $\chi^2$  distribution [41, Ch.2.2] and therefore the statistic of the normalized amplitude measurement  $z_{\text{u}m,n}$  by a Rician distribution. However, the proof and the details are out-of-scope of this paper.

$$= \left[ \begin{array}{ccc} \frac{\Re\{\tilde{\alpha}_{l,n}\} \|\mathbf{s}(\tilde{\theta}_{l,n})\|}{|\tilde{\alpha}_{l,n}| \sigma} & \frac{\Im\{\tilde{\alpha}_{l,n}\} \|\mathbf{s}(\tilde{\theta}_{l,n})\|}{|\tilde{\alpha}_{l,n}| \sigma} & \frac{-|\tilde{\alpha}_{l,n}| \|\mathbf{s}(\tilde{\theta}_{l,n})\|}{2\sigma^3} \end{array} \right]^T. \quad (59)$$

Note that the second term  $\frac{\tilde{u}_{l,n}^2}{4N_s H}$  in (58) characterizes the effect of the noise variance estimation, which becomes significant for high component SNRs, and converges to zero for low component SNRs or a high number of samples. Thus, for *PMPC-oriented* measurements the spread parameter of the Rician likelihood function in (9) is given by (58) and for false alarm measurements the spread of 1/2 is used in the Rayleigh likelihood function.

## REFERENCES

- [1] M. L. Jakobsen, T. Pedersen, and B. H. Fleury, “Analysis of stochastic radio channels with temporal birth-death dynamics: A marked spatial point process perspective,” *IEEE Trans. Antennas Propag.*, vol. 62, no. 7, pp. 3761–3775, Apr. 2014.
- [2] J. Flordelis, X. Li, O. Edfors, and F. Tufvesson, “Massive MIMO extensions to the COST 2100 channel model: Modeling and validation,” *IEEE Trans. Wireless Commun.*, vol. 19, no. 1, pp. 380–394, Oct. 2020.
- [3] F. Rusek, D. Persson, B. K. Lau, E. G. Larsson, T. L. Marzetta, O. Edfors, and F. Tufvesson, “Scaling up MIMO: Opportunities and challenges with very large arrays,” *IEEE Signal Process. Mag.*, vol. 30, no. 1, pp. 40–60, Jan. 2013.
- [4] R. Di Taranto, S. Muppuru, R. Raulefs, D. Slock, T. Svensson, and H. Wymeersch, “Location-aware communications for 5G networks: How location information can improve scalability, latency, and robustness of 5G,” *IEEE Signal Process. Mag.*, vol. 31, no. 6, pp. 102–112, Nov. 2014.
- [5] S. Hu, F. Rusek, and O. Edfors, “Beyond massive MIMO: The potential of data transmission with large intelligent surfaces,” *IEEE Trans. Signal Process.*, vol. 66, no. 10, pp. 2746–2758, May 2018.
- [6] C. Gentner, T. Jost, W. Wang, S. Zhang, A. Dammann, and U. C. Fiebig, “Multipath assisted positioning with simultaneous localization and mapping,” *IEEE Trans. Wireless Commun.*, vol. 15, no. 9, pp. 6104–6117, Sept. 2016.
- [7] E. Leitinger, F. Meyer, F. Tufvesson, and K. Witrisal, “Factor graph based simultaneous localization and mapping using multipath channel information,” in *Proc. IEEE ICCW-17*, Paris, France, May 2017, pp. 652–658.
- [8] E. Leitinger, F. Meyer, F. Hlawatsch, K. Witrisal, F. Tufvesson, and M. Z. Win, “A belief propagation algorithm for multipath-based SLAM,” *IEEE Trans. Wireless Commun.*, vol. 18, no. 12, pp. 5613–5629, Dec. 2019.
- [9] R. Mendrzik, F. Meyer, G. Bauch, and M. Z. Win, “Enabling situational awareness in millimeter wave massive MIMO systems,” *IEEE J. Sel. Topics Signal Process.*, vol. 13, no. 5, pp. 1196–1211, Sept. 2019.
- [10] R. Schmidt, “Multiple emitter location and signal parameter estimation,” *IEEE Trans. Antennas Propag.*, vol. 34, no. 3, pp. 276–280, Mar. 1986.
- [11] R. Roy and T. Kailath, “ESPRIT-estimation of signal parameters via rotational invariance techniques,” *IEEE Trans. Acoust., Speech, Signal Process.*, vol. 37, no. 7, pp. 984–995, Jul. 1989.
- [12] M. Haardt, F. Roemer, and G. Del Galdo, “Higher-order SVD-based subspace estimation to improve the parameter estimation accuracy in multidimensional harmonic retrieval problems,” *IEEE Trans. Signal Process.*, vol. 56, no. 7, pp. 3198–3213, June 2008.
- [13] B. Ottersten, M. Viberg, P. Stoica, and A. Nehorai, “Exact and large sample maximum likelihood techniques for parameter estimation and detection in array processing,” in *Radar Array Processing*. Springer, 1993, pp. 99–151.
- [14] J. A. Fessler and A. O. Hero, “Space-alternating generalized expectation-maximization algorithm,” *IEEE Trans. Signal Process.*, vol. 42, no. 10, pp. 2664–2677, Oct. 1994.

- [15] B. H. Fleury, M. Tschudin, R. Heddergott, D. Dahlhaus, and K. Ingeman Pedersen, “Channel parameter estimation in mobile radio environments using the SAGE algorithm,” *IEEE J. Sel. Areas Commun.*, vol. 17, no. 3, pp. 434–450, 1999.
- [16] A. Richter, “Estimation of radio channel parameters: Models and algorithms,” Ph.D. dissertation, Ilmenau University of Technology, 2005.
- [17] P. Stoica and Y. Selen, “Model-order selection: a review of information criterion rules,” *IEEE Signal Process. Mag.*, vol. 21, no. 4, pp. 36–47, Jul. 2004.
- [18] D. Shutin and B. H. Fleury, “Sparse variational Bayesian SAGE algorithm with application to the estimation of multipath wireless channels,” *IEEE Trans. Signal Process.*, vol. 59, no. 8, pp. 3609–3623, Aug. 2011.
- [19] M. A. Badiu, T. L. Hansen, and B. H. Fleury, “Variational Bayesian inference of line spectra,” *IEEE Trans. Signal Process.*, vol. 65, no. 9, pp. 2247–2261, May 2017.
- [20] T. L. Hansen, B. H. Fleury, and B. D. Rao, “Superfast line spectral estimation,” *IEEE Trans. Signal Process.*, vol. PP, no. 99, pp. 1–1, 2018.
- [21] S. Grebien, E. Leitinger, K. Witrisal, and B. H. Fleury, “Super-resolution channel estimation including the dense multipath component — A sparse Bayesian approach,” 2021, in preparation.
- [22] J. Salmi, A. Richter, and V. Koivunen, “Detection and tracking of MIMO propagation path parameters using state-space approach,” *IEEE Trans. Signal Process.*, vol. 57, no. 4, pp. 1538–1550, Apr. 2009.
- [23] X. Li, E. Leitinger, M. Oskarsson, K. Åström, and F. Tufvesson, “Massive MIMO-based localization and mapping exploiting phase information of multipath components,” *IEEE Trans. Wireless Commun.*, vol. 18, no. 9, pp. 4254–4267, Sept. 2019.
- [24] D. Shutin and B. Vexler, “Sparse Bayesian learning with dictionary refinement for super-resolution through time,” in *Proc. IEEE CAMSAP-17*, Dec. 2017, pp. 1–5.
- [25] T. Jost, W. Wang, U. Fiebig, and F. Perez-Fontan, “Detection and tracking of mobile propagation channel paths,” *IEEE Trans. Antennas Propag.*, vol. 60, no. 10, pp. 4875–4883, Oct. 2012.
- [26] Y. Bar-Shalom, P. K. Willett, and X. Tian, *Tracking and data fusion: a handbook of algorithms*. Storrs, CT, USA: Yaakov Bar-Shalom, 2011.
- [27] F. Meyer, T. Kropfreiter, J. L. Williams, R. Lau, F. Hlawatsch, P. Braca, and M. Z. Win, “Message passing algorithms for scalable multitarget tracking,” *Proc. IEEE*, vol. 106, no. 2, pp. 221–259, Feb. 2018.
- [28] F. Meyer and J. L. Williams, “Scalable detection and tracking of geometric extended objects,” 2021, arXiv:2103.11279.
- [29] F. Meyer and K. L. Gemba, “Probabilistic focalization for shallow water localization,” *J. Acoust. Soc. Am.*, 2021.
- [30] F. Meyer, P. Braca, P. Willett, and F. Hlawatsch, “A scalable algorithm for tracking an unknown number of targets using multiple sensors,” *IEEE Trans. Signal Process.*, vol. 65, no. 13, pp. 3478–3493, July 2017.
- [31] D. Lerro and Y. Bar-Shalom, “Automated tracking with target amplitude information,” in *1990 American Control Conf.*, May 1990, pp. 2875–2880.
- [32] E. Leitinger, S. Grebien, X. Li, F. Tufvesson, and K. Witrisal, “On the use of MPC amplitude information in radio signal based SLAM,” in *Proc. IEEE SSP-18*, Freiburg, Germany, June 2018, pp. 633–637.
- [33] E. Leitinger, S. Grebien, and K. Witrisal, “Multipath-based SLAM exploiting AoA and amplitude information,” in *Proc. IEEE ICCW-19*, Shanghai, China, May 2019, pp. 1–7.
- [34] G. Soldi, F. Meyer, P. Braca, and F. Hlawatsch, “Self-tuning algorithms for multisensor-multitarget tracking using belief propagation,” *IEEE Trans. Signal Process.*, vol. 67, no. 15, pp. 3922–3937, Aug. 2019.
- [35] D. Shutin, W. Wang, and T. Jost, “Incremental sparse bayesian learning for parameter estimation of superimposed signals,” in *Proc. SAMPTA-2013*, no. 1, Sept. 2013, pp. 6–9.
- [36] T. Wilding, S. Grebien, E. Leitinger, U. Mühlmann, and K. Witrisal, “Single-anchor, multipath-assisted indoor positioning with aliased antenna arrays,” in *Asilomar-18*, Pacific Grove, CA, USA, Oct. 2018, pp. 525–531.
- [37] A. F. Molisch, *Wireless Communications*, 2nd ed. New York, USA: Wiley Publishing, 2011.

- [38] J. Williams and R. Lau, "Approximate evaluation of marginal association probabilities with belief propagation," *IEEE Trans. Aerosp. Electron. Syst.*, vol. 50, no. 4, pp. 2942–2959, Oct. 2014.
- [39] F. Kschischang, B. Frey, and H.-A. Loeliger, "Factor graphs and the sum-product algorithm," *IEEE Trans. Inf. Theory*, vol. 47, no. 2, pp. 498–519, Feb. 2001.
- [40] H.-A. Loeliger, "An introduction to factor graphs," *IEEE Signal Process. Mag.*, vol. 21, no. 1, pp. 28–41, Feb. 2004.
- [41] S. M. Kay, *Fundamentals of Statistical Signal Processing: Detection Theory*. Upper Saddle River, NJ, USA: Prentice Hall, 1998.
- [42] S. M. Kay, *Fundamentals of Statistical Signal Processing: Estimation Theory*. Upper Saddle River, NJ, USA: Prentice-H, 1993.
- [43] F. Meyer, O. Hlinka, H. Wymeersch, E. Riegler, and F. Hlawatsch, "Distributed localization and tracking of mobile networks including noncooperative objects," *IEEE Trans. Signal Inf. Process. Net.*, vol. 2, no. 1, pp. 57–71, Mar. 2016.
- [44] P. Tichavsky, C. Muravchik, and A. Nehorai, "Posterior Cramer-Rao bounds for discrete-time nonlinear filtering," *IEEE Trans. Signal Process.*, vol. 46, no. 5, pp. 1386–1396, May 1998.
- [45] Y. Bar-Shalom, T. Kirubarajan, and X.-R. Li, *Estimation with Applications to Tracking and Navigation*. New York, NY, USA: Wiley, 2002.
- [46] D. Schuhmacher, B.-T. Vo, and B.-N. Vo, "A consistent metric for performance evaluation of multi-object filters," *IEEE Trans. Signal Process.*, vol. 56, no. 8, pp. 3447–3457, Aug. 2008.
- [47] E. Leitinger, S. Grebien, B. H. Fleury, and K. Witrisal, "Detection and estimation of a spectral line in MIMO systems," in *Proc. Asilomar-20*, Pacific Grove, CA, USA, Oct. 2020, pp. 1090–1095.
- [48] P. Meissner, "Multipath-assisted indoor positioning," Ph.D. dissertation, Graz University of Technology, 2014.
- [49] H. L. Van Trees, *Detection, Estimation and Modulation, Part I*. Wiley Press, 1968.
- [50] K. J. Worsley, "Local maxima and the expected euler characteristic of excursion sets of  $\chi^2$ , f and t fields," *Adv. Appl. Probab.*, vol. 26, no. 1, pp. 13–42, 1994. [Online]. Available: <http://www.jstor.org/stable/1427576>
- [51] R. J. Adler and J. E. Taylor, *Random Fields and Geometry*. New York, NY, USA: Springer, 2007.
- [52] R. J. Adler, J. E. Taylor, and K. J. Worsley, "Applications of random fields and geometry: Foundations and case studies," 2015, in preparation.